UNIVERSIDAD POLITÉCNICA DE MADRID

ESCUELA TÉCNICA SUPERIOR DE INGENIERÍA AERONÁUTICA Y DEL ESPACIO

SSECOID
Stability and Sensitivity Methods for Flow Control and Industrial Design

DLR

INSTABILITY MECHANISMS IN CROSSFLOW-DOMINATED SWEPT-WING BOUNDARY LAYERS WITH SURFACE IRREGULARITIES

Candidate : Biagio Ambrosino
Supervisor : Stefan Hein
Co-supervisor: Daniel Rodríguez

PhD Defense: 24/09/2026

SSeCoID : Stability and Sensitivity Methods for Flow Control and Industrial Design

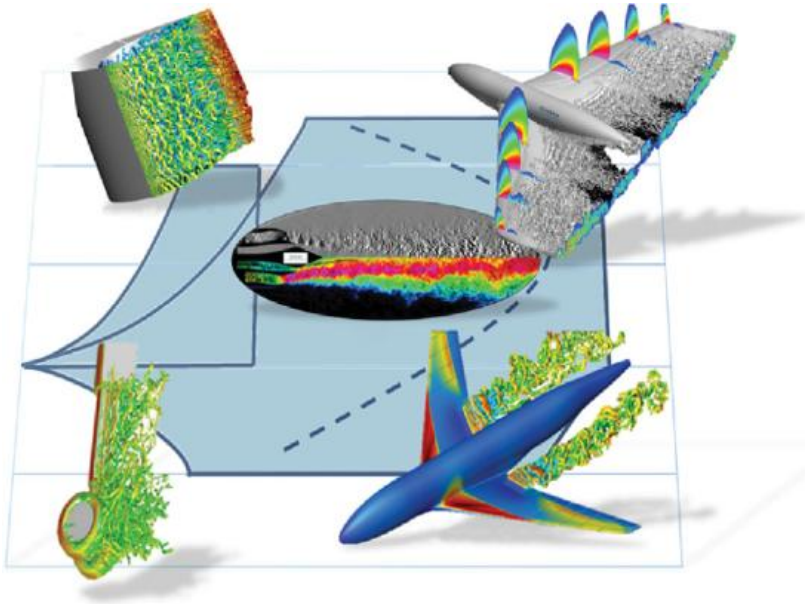
- Duration: 48 months. (Jan 2021- Dec 2024)

- Participating institutions: **DLR**, ONERA, ICL, UCAM, UPM, VKI, KTH, KULEUVEN, CIMNE, PURDUE, XAAR, SDSU, CADENCE, AIRBUS ES, MCLAREN RACING.

- Funding: European Union's Horizon 2020 research and innovation program under grant agreement No: 955923.

- MARIE SKŁODOWSKA-CURIE ACTIONS (MSCA) Innovative Training Networks (ITN) Call: H2020-MSCA-ITN-2020.

- Training of 15 researchers in the development of most advanced methods for simulation, stability and flow control techniques applied to industrial design.



Outline

From crossflow instability to the effect of surface irregularities

1 **Motivation**

Crossflow-dominated transition

2 **Methodology**

DNS · LST-2D · PSE-3D

3 **Clean surface**

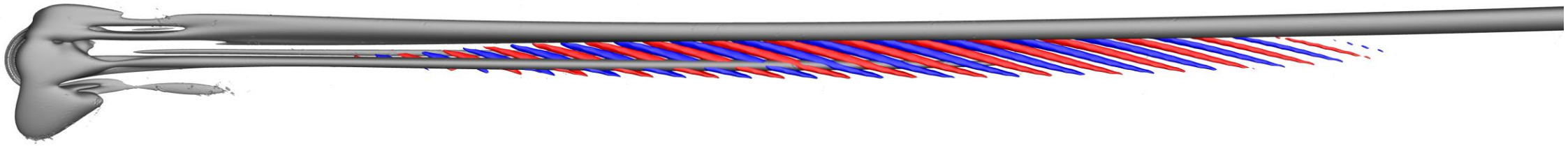
Validation & secondary instability

4 **Surface irregularities**

- Smooth humps
- Forward-facing steps
- Cylindrical roughness

5 **Synthesis**

Conclusions & outlook



Motivation

Why laminar-turbulent transition matters for swept-wing aerodynamics



Lower aircraft drag

Extending laminar flow over aerodynamic surfaces can lead to a **significant reduction** of aircraft drag.

Transition prediction

A fundamental challenge for the design of laminar wings is the **understanding** and **reliable prediction** of the laminar–turbulent transition process.

Focus of this thesis

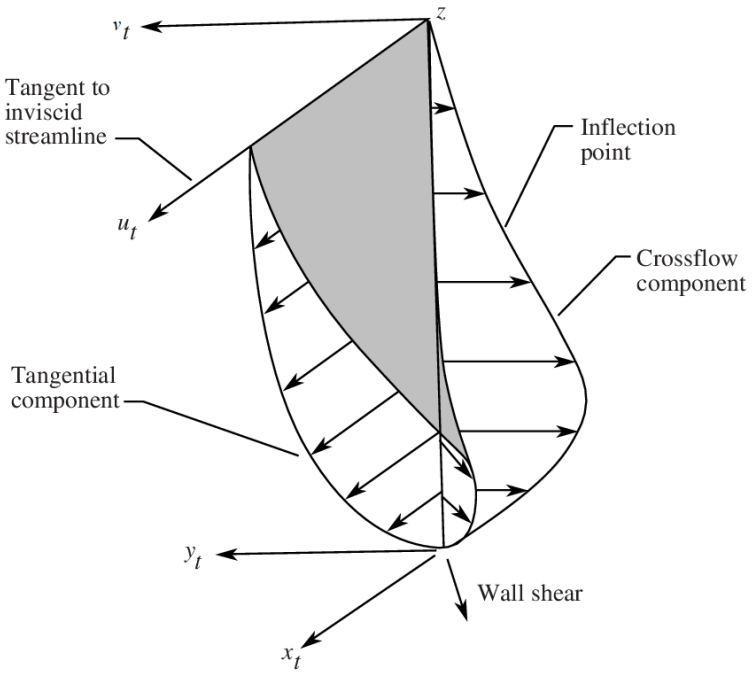
Focus on the transition process in **three-dimensional** boundary layers of swept wings.



Understanding and controlling transition is a key enabler for laminar-wing design.

Origin of crossflow instability

Physical mechanism driving crossflow in swept-wing boundary layers



Saric et al., Annual Review of Fluid Mechanics 2003 35:1, 413-440

1 **Curvature → Force balance**

Curved external streamlines generate centrifugal forces, balanced by the pressure forces outside the boundary layer.

2 **Viscosity → Force imbalance**

Toward the wall, velocity and centrifugal forces decrease, while the pressure field remains approximately unchanged.

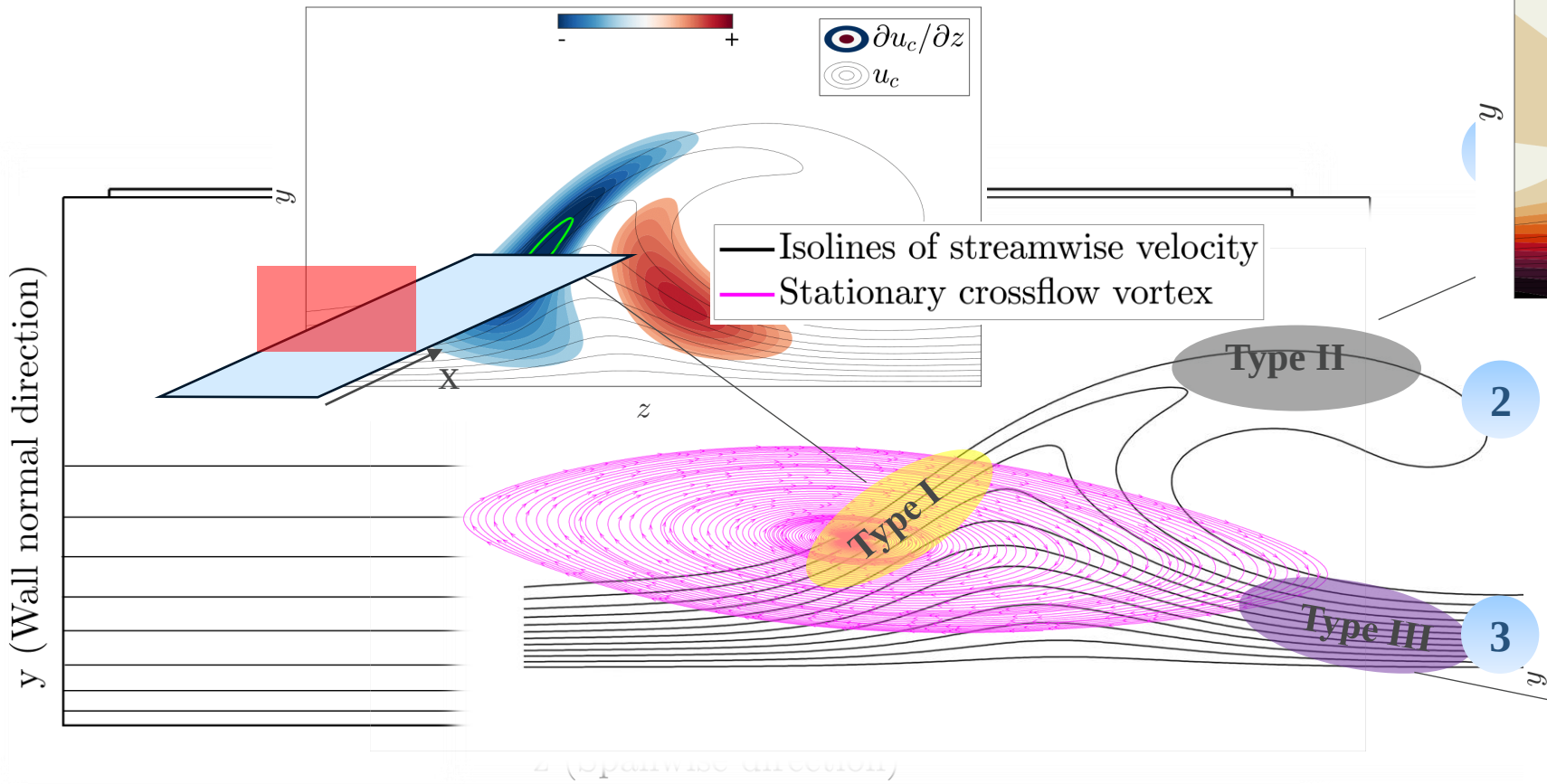
3 **Imbalance → Crossflow instability**

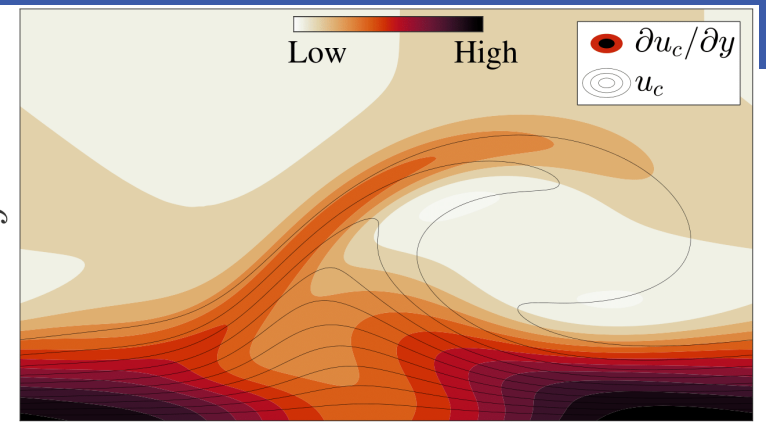
The imbalance drives a spanwise velocity component: crossflow. The profile is inflectional and susceptible to instability.

At low freestream turbulence, stationary crossflow vortices can dominate — how do they trigger breakdown?

Secondary instability of finite-amplitude stationary crossflow vortices

From primary crossflow to breakdown

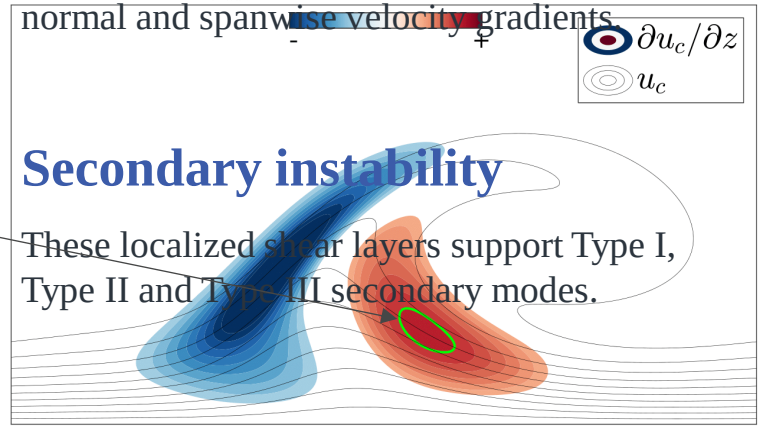




2

Strong shear layers

The distorted base flow develops strong wall-normal and spanwise velocity gradients.



3

Secondary instability

These localized shear layers support Type I, Type II and Type III secondary modes.

Surface irregularities in swept-wing boundary layers

Real surfaces can strongly modify instability growth and transition



Realistic surfaces

Manufacturing tolerances, waviness, steps, roughness and surface wear are unavoidable in practice.

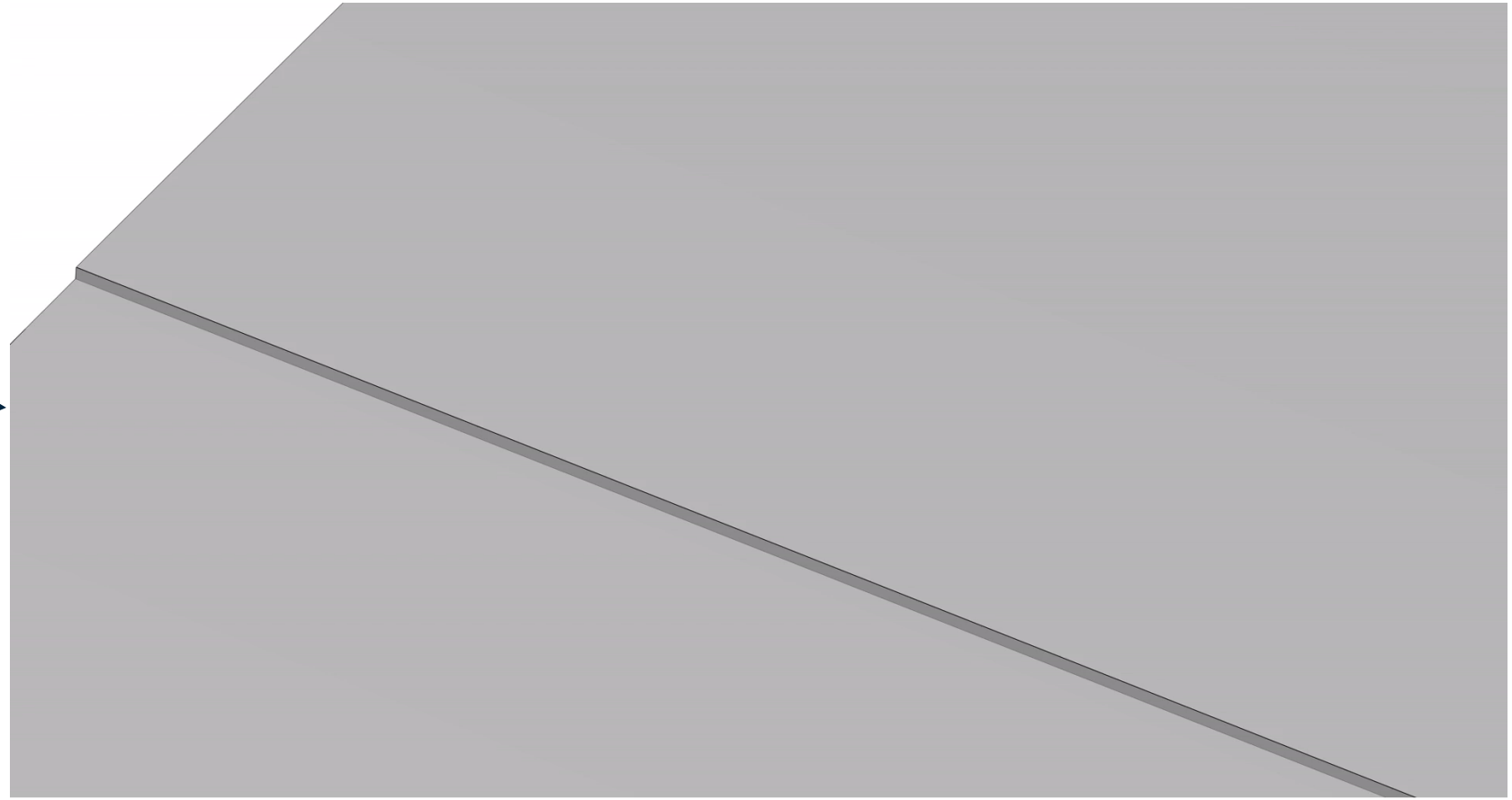
Prediction challenge

Even small surface features can distort the base flow, modify instability growth and shift transition.

Surface irregularities in swept-wing boundary layers

Real surfaces can strongly modify instability growth and transition





Thesis objectives

From the physics of secondary instability to the effect of surface irregularities

Motivation/ Research gap

Predicting secondary instabilities of stationary crossflow vortices remains uncertain, with discrepancies reported between linear stability analysis and DNS.

Systematic studies of how surface irregularities modify these instabilities in three-dimensional swept-wing boundary layers remain scarce.

1 Understand the instability physics

Characterise the evolution and amplification of secondary instabilities of stationary crossflow vortices.

2 Develop and validate stability analysis tools

Assess LST-2D and PSE-3D against DNS for three-dimensional boundary layers.

3 Quantify the role of surface irregularities

Determine how surface irregularities modify instability mechanisms and transition.

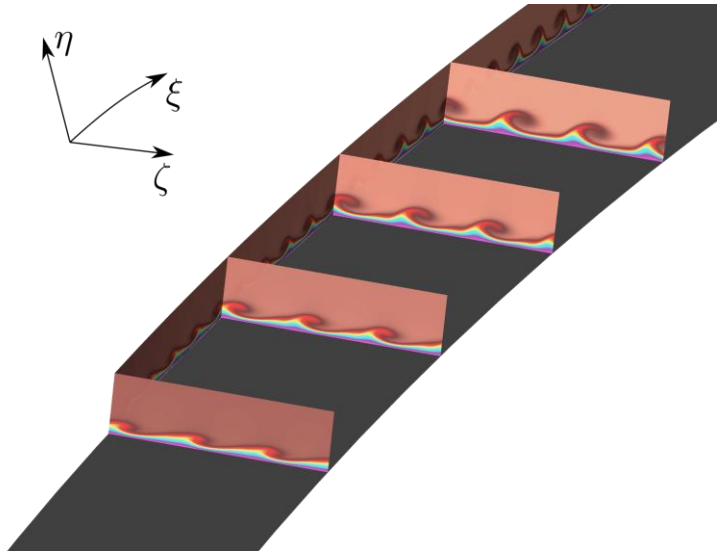
How do surface irregularities modify the instability mechanisms that ultimately lead to transition in crossflow-dominated boundary layers?

Methodological framework

DNS and linear stability analysis for identifying and validating instability mechanisms

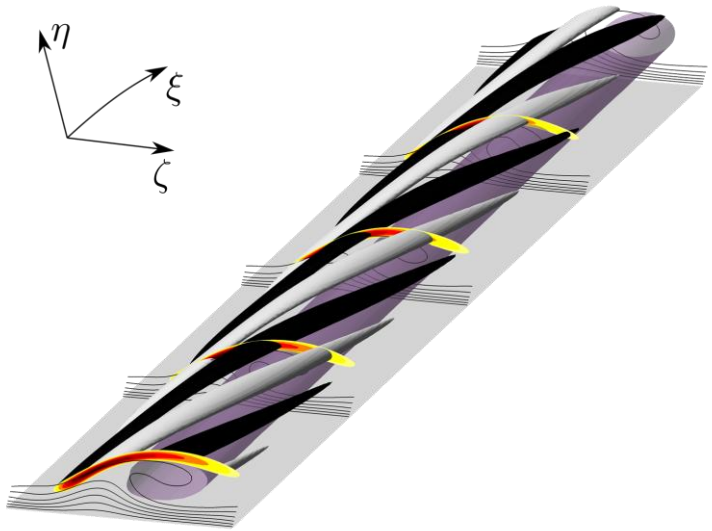
1 Base flow

DNS



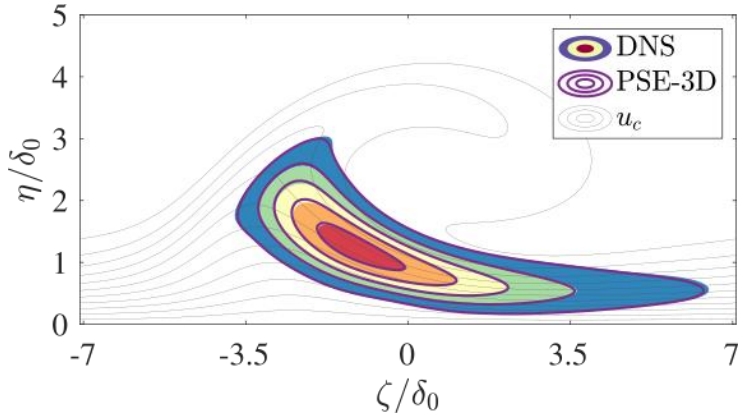
2 Linear stability analysis

LST-2D + PSE-3D



3 Validation and comparison

Linear stability ↔ DNS



Direct numerical simulation

High-fidelity reference for the base flow and disturbance evolution

GOVERNING EQUATION

Incompressible Navier-Stokes

The equations are solved directly, without a turbulence model.

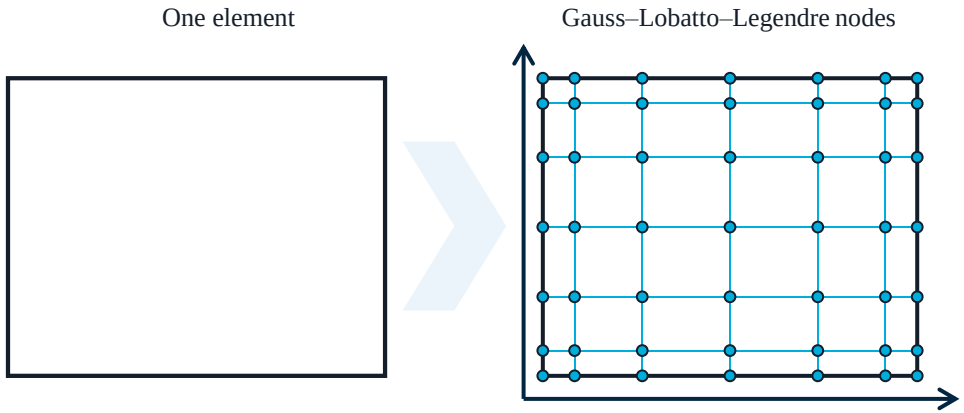
$$\nabla \cdot u = 0,$$

$$\partial u/\partial t + u \cdot \nabla u = -\nabla p + (1/Re)\,\nabla^2 u.$$

SPECTRAL-ELEMENT METHOD

Nek5000

- Domain decomposed into hexahedral elements
- High-order polynomial representation inside each element
- $P_n - P_{n-2}$ velocity–pressure formulation



DNS provides the steady three-dimensional base flow and the unsteady reference disturbances.

Linear stability framework

From the base flow to a mathematical description of disturbance evolution

1 Flow decomposition

The instantaneous flow is decomposed into an undisturbed basic state and a small-amplitude perturbation.

$$\boldsymbol{q}(\boldsymbol{\xi}, t) = \overline{\boldsymbol{q}}(\xi) + \varepsilon\widetilde{\boldsymbol{q}}(\boldsymbol{\xi}, t)$$

$\overline{q}$ **base flow** $\widetilde{q}$ **perturbation**

→

2 Linearization

Insert the decomposition into the Navier–Stokes equations and neglect products of perturbation quantities.

$$L(\overline{\boldsymbol{q}})\widetilde{\boldsymbol{q}} = 0$$

Linearized Navier–Stokes equations

→

3 Disturbance representation

The disturbance is expressed as an amplitude function multiplied by a rapidly varying phase function.

$$\widetilde{\boldsymbol{q}} = \widehat{\boldsymbol{q}}\, e^{i\boldsymbol{\Theta}}$$

$\widehat{q}$ **amplitude** $\boldsymbol{\Theta}$ **phase**

Linear stability analysis describes the evolution of small disturbances superimposed on a steady base flow.

Linear stability approaches

Local and *non-local* stability methodologies

Local linear stability analysis

$$\partial\bar{q}/\partial x = 0$$

LST-2D: $\bar{q} = \bar{q}(y,z)$

$\tilde{q}(x,y,z,t) = \hat{q}(y,z)e^{i\Theta}$

$\Theta = \alpha x - \omega t$

Base flow inhomogeneous in the spanwise direction (z)

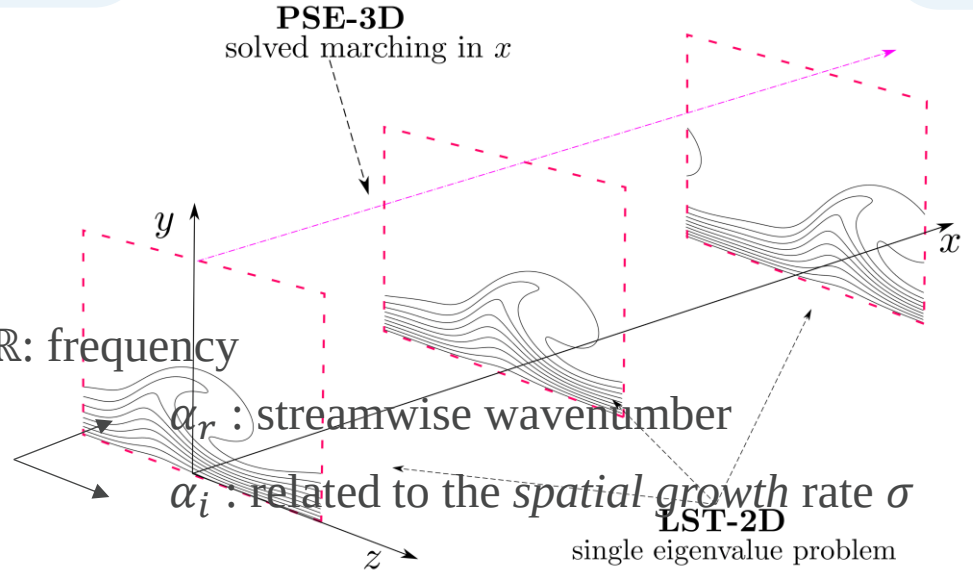
Non-local linear stability analysis

$$\partial\bar{q}/\partial x \ll \partial\bar{q}/\partial y, \partial\bar{q}/\partial z$$

PSE-3D: $\bar{q} = \bar{q}(x_s, y, z)$

$\tilde{q}(x,y,z,t) = \hat{q}(x_s,y,z)e^{i\Theta}$

$\Theta = \int_{x_0}^{x} \alpha(x')dx' - \omega t$



Spatial theory

- $\omega \in \mathbb{R}$: frequency
- $\alpha \in \mathbb{C}$

α_r : streamwise wavenumber

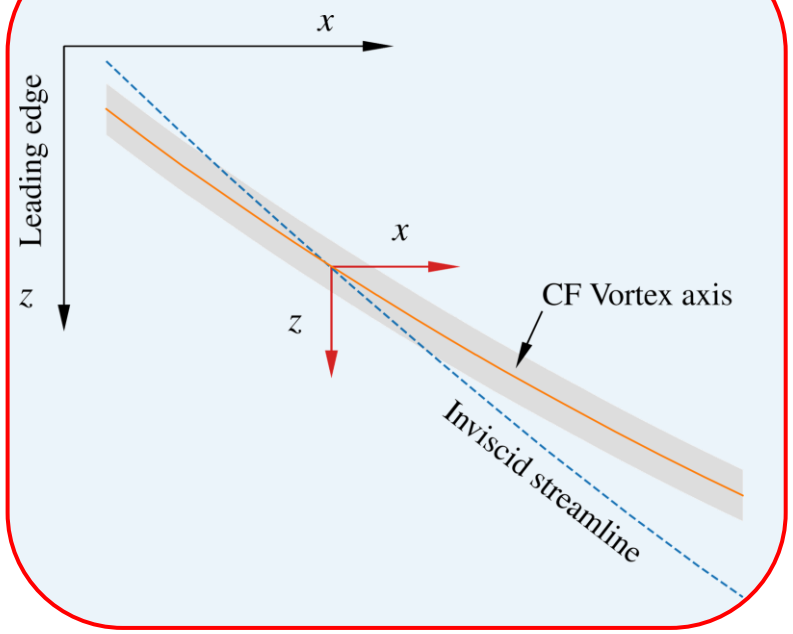
α_i : related to the *spatial growth* rate σ

N-factor: $N = \int_{x_0}^{x} \sigma \, dx'$

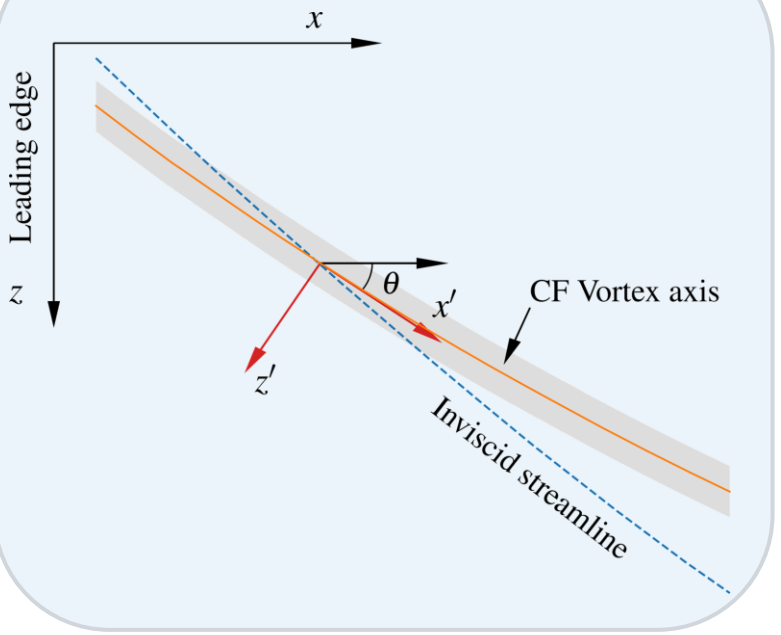
Choice of the coordinate system

Out-of-plane direction chosen to align along the one of least variation

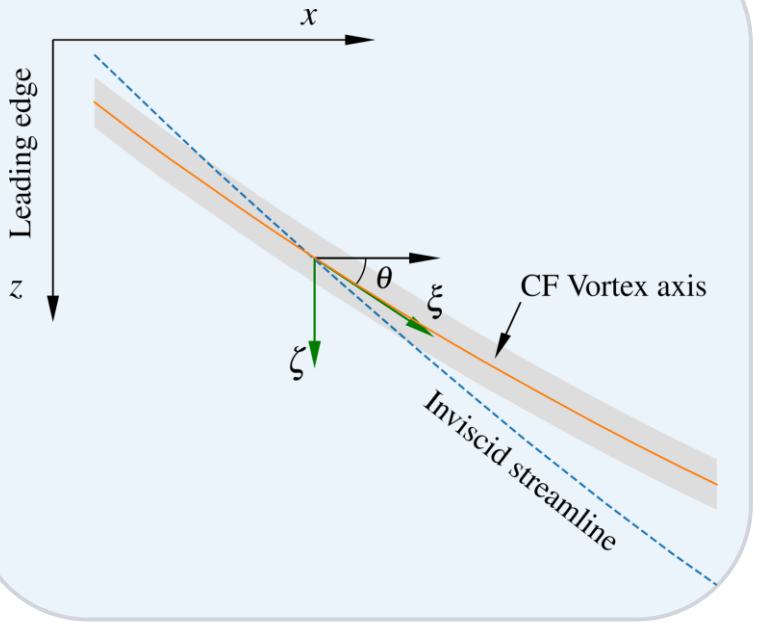
ORTHOGONAL



VORTEX-ORIENTED



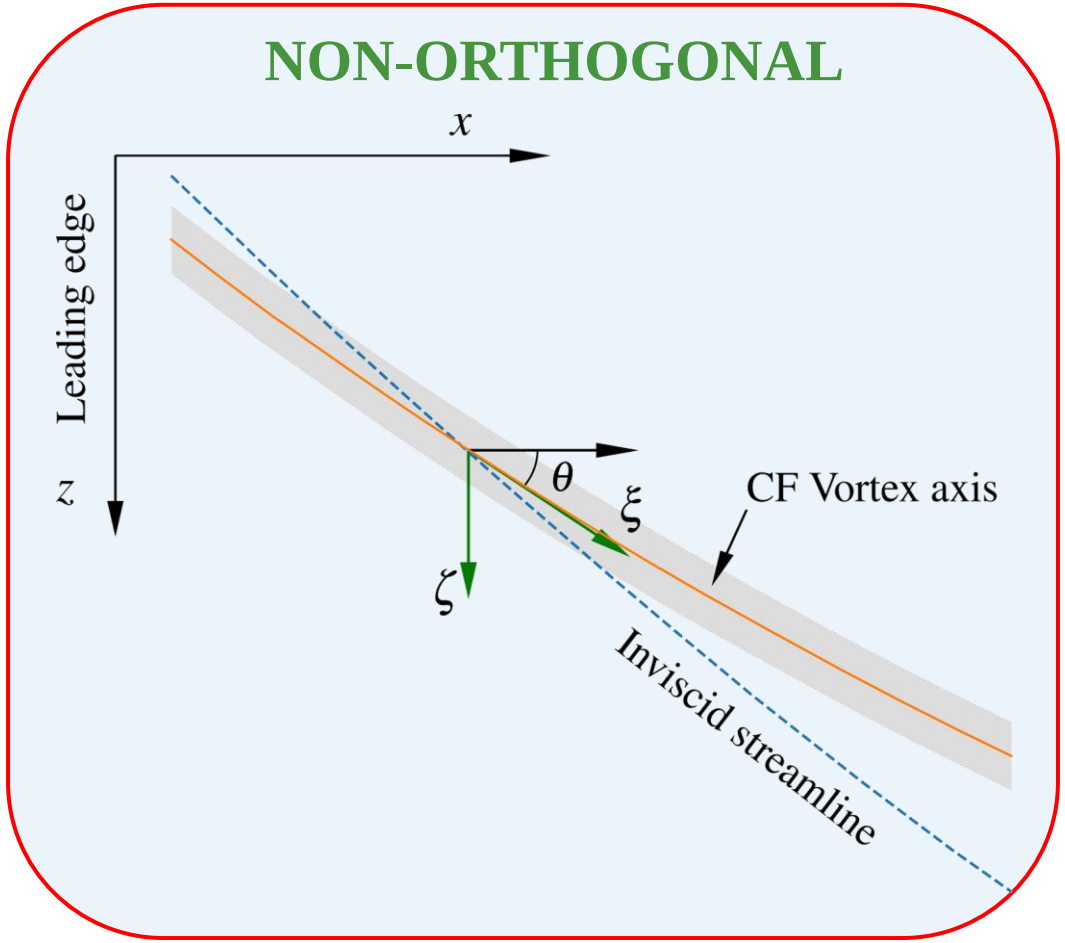
NON-ORTHOGONAL



The non-orthogonal system fulfills spanwise periodicity and minimizes the out-of-plane variation of the base flow.

Choice of the coordinate system

Out-of-plane direction chosen to align along the one of least variation



The non-orthogonal system fulfills spanwise periodicity and minimizes the out-of-plane variation of the base flow.

Equations in generalized curvilinear coordinate system

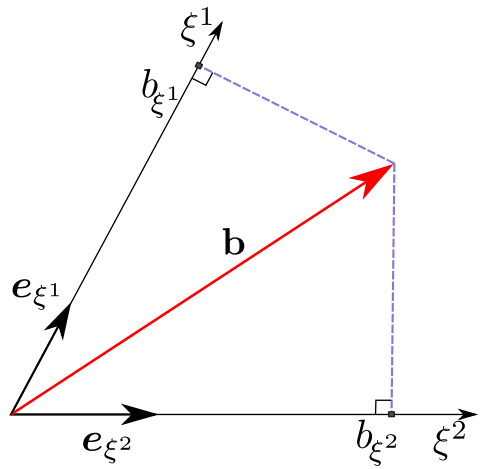
Covariant and contravariant vector representation

$$b_i = g_{ij}\, b^j \qquad b^i = g^{ij}\, b_j$$

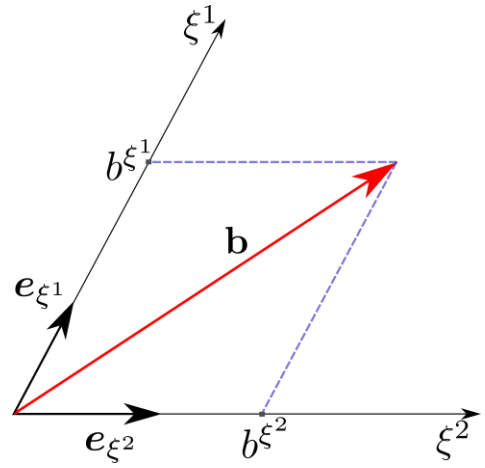
$$g^{ij} = \sum_k \frac{\partial y^k}{\partial x^i}\frac{\partial y^k}{\partial x^j} = \begin{pmatrix} g^{11} & g^{12} & g^{13} \\ g^{21} & g^{22} & g^{23} \\ g^{31} & g^{32} & g^{33} \end{pmatrix}$$

y^i represents the Cartesian coordinate system and x^i a general curvilinear coordinate system.

GEOMETRIC INTERPRETATION



COVARIANT COMPONENTS



CONTRAVARIANT COMPONENTS

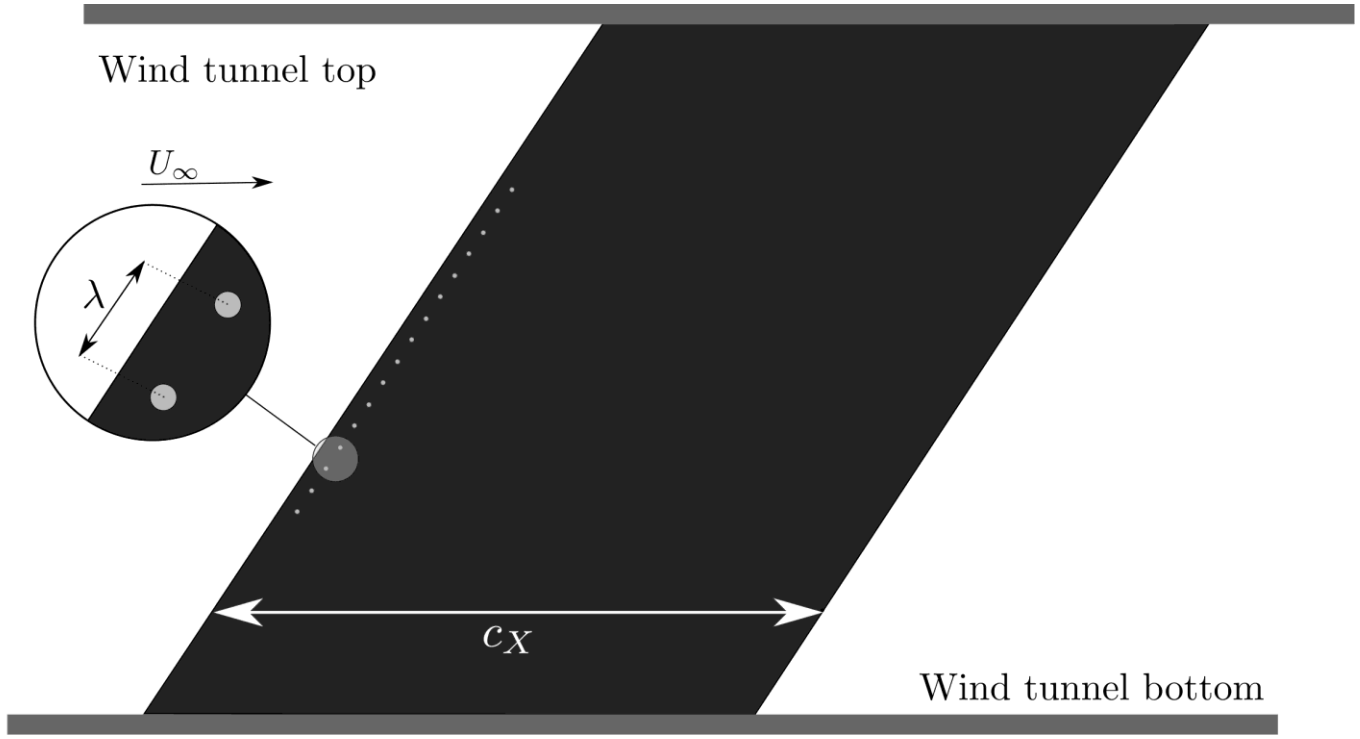
In a non-orthogonal basis the two component sets are different, even though they represent the same physical vector.

Contravariant components are used throughout the stability formulation.

Reference swept-wing configuration

Controlled stationary-crossflow case used to validate the stability framework

EXPERIMENTAL CONFIGURATION



REFERENCE CONDITIONS

Parameter	Value
c_X	1.27 m
Λ	45°
AoA	-3°
U_∞	27.5 ms^{-1}
Re_{c_X}	2.37×10^6
λ_z	7.5 mm
δ_0	5.25×10^{-4} m

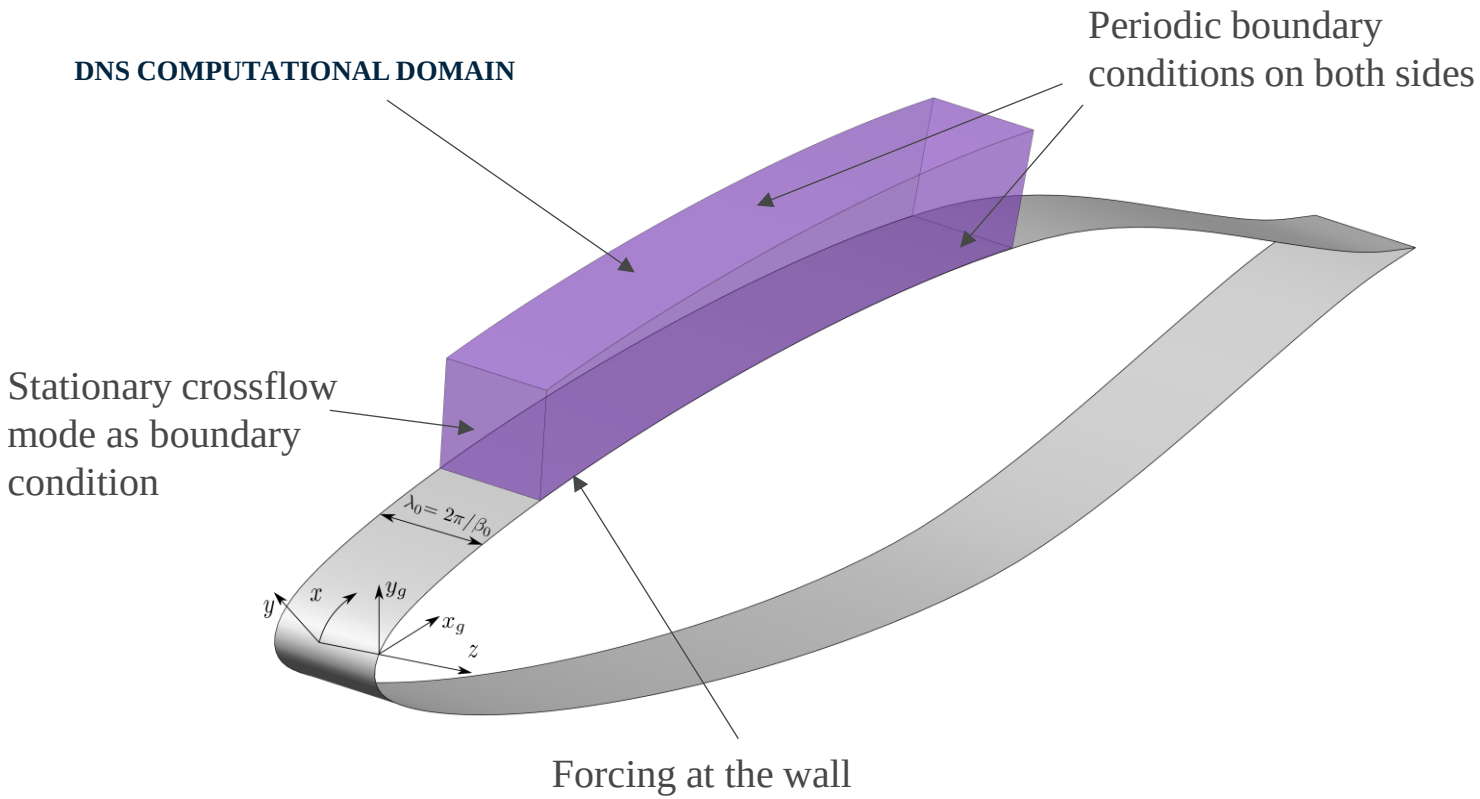
Based on the TU Delft swept-wing experiment.

Rius-Vidales & Kotsonis, JFM 924:34 (2021)

A controlled stationary crossflow vortex provides the baseline for DNS–stability comparison.

DNS setup

Generation of the finite-amplitude stationary crossflow vortex in DNS



1 Stationary crossflow mode

A single stationary mode is imposed, matching the experimentally forced spanwise wavelength.

2 Spanwise periodicity

Periodic lateral boundaries reproduce one wavelength of the stationary vortex.

3 Localized forcing

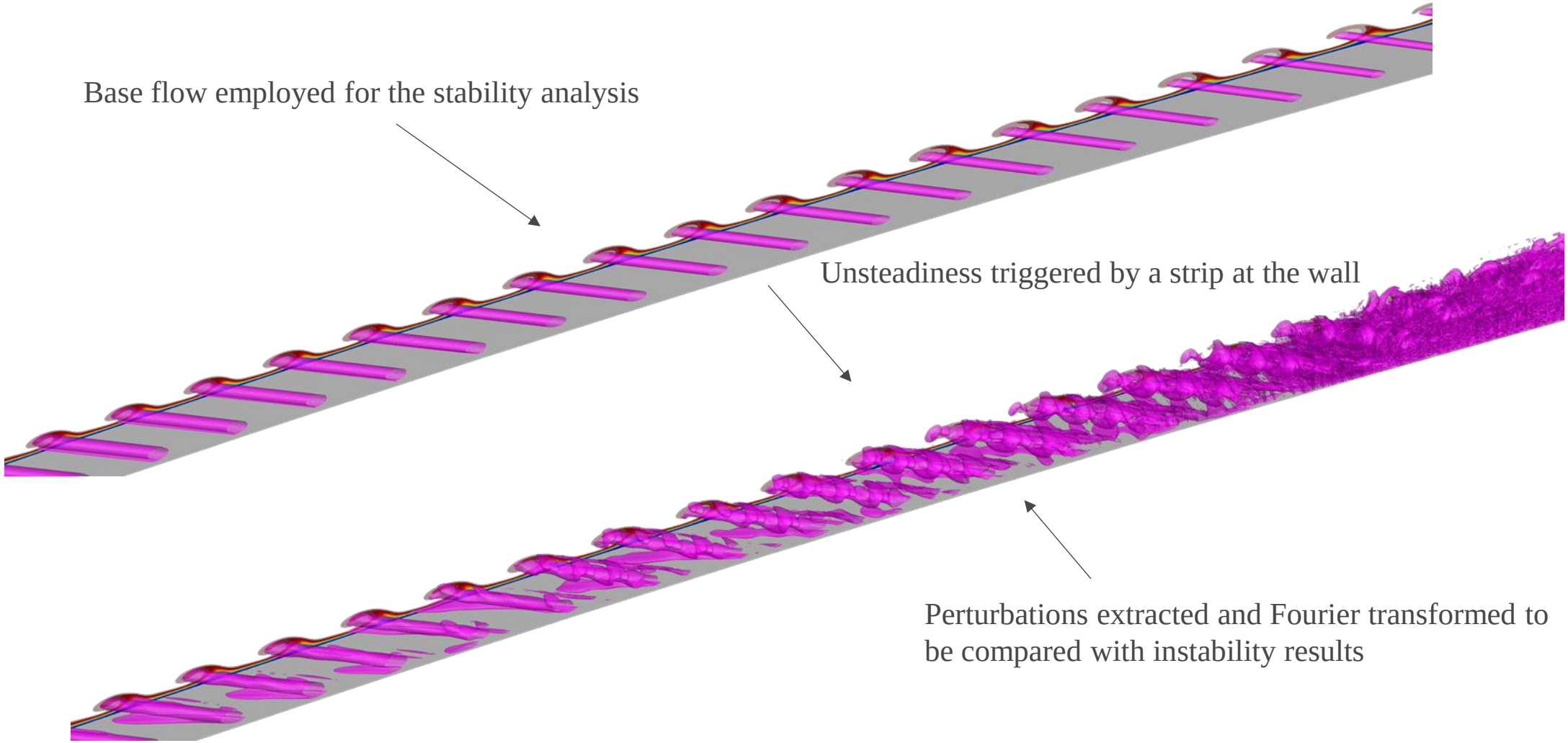
A localized trip/forcing strip is used at the wall.

The DNS reproduces the experimental configuration and provides the 3-D base flow for stability analysis.

Data note: the DNS database used in this work was provided by Francesco Tocci (DLR Göttingen).

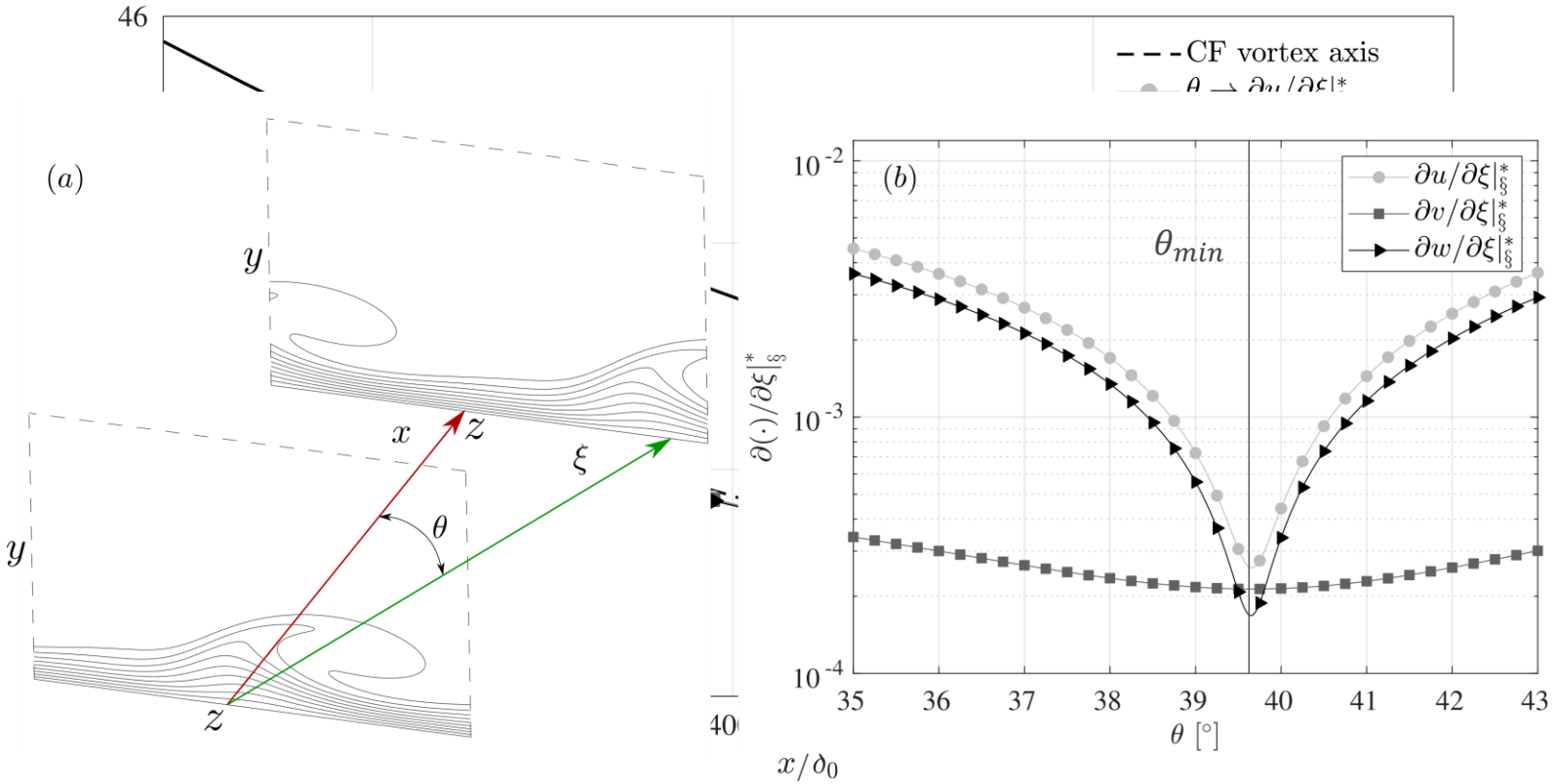
DNS results

Steady base flow and unsteady disturbance field



Direction of least base-flow variation

The direction of minimum base-flow variation closely aligns with the crossflow-vortex axis



1 Measure variation

Compute the RMS of the out-of-plane derivative in each $y-z$ plane.

2 Find minimum angle

Vary the direction angle and select the minimum for the velocity components u, v and w.

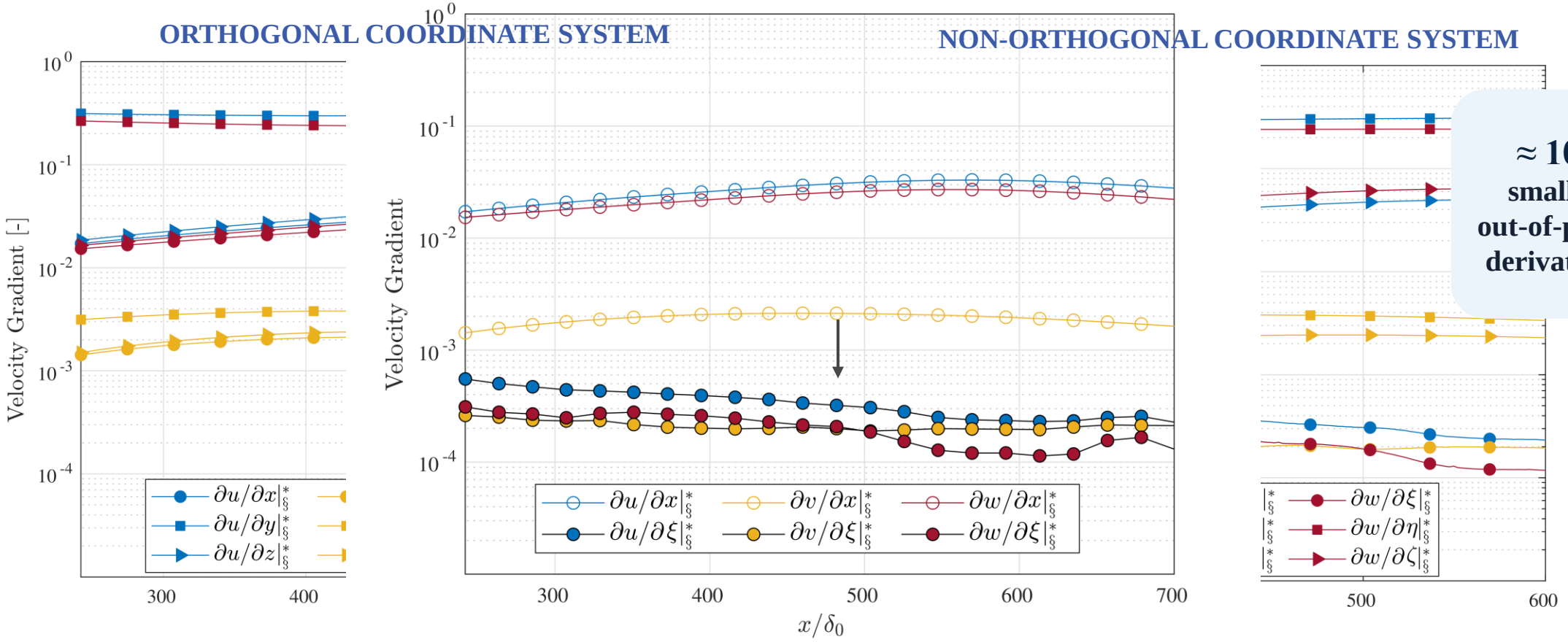
$$\theta_{\min,u} \approx \theta_{\min,v} \approx \theta_{\min,w}$$

$$\theta_{min} \approx \theta_{CF_{\text{vortex}}}$$

The crossflow-vortex provides a physical measure of the direction along which the 3D base flow varies the least.

Impact of coordinate-system orientation

Quantifying the reduction in out-of-plane base-flow variation

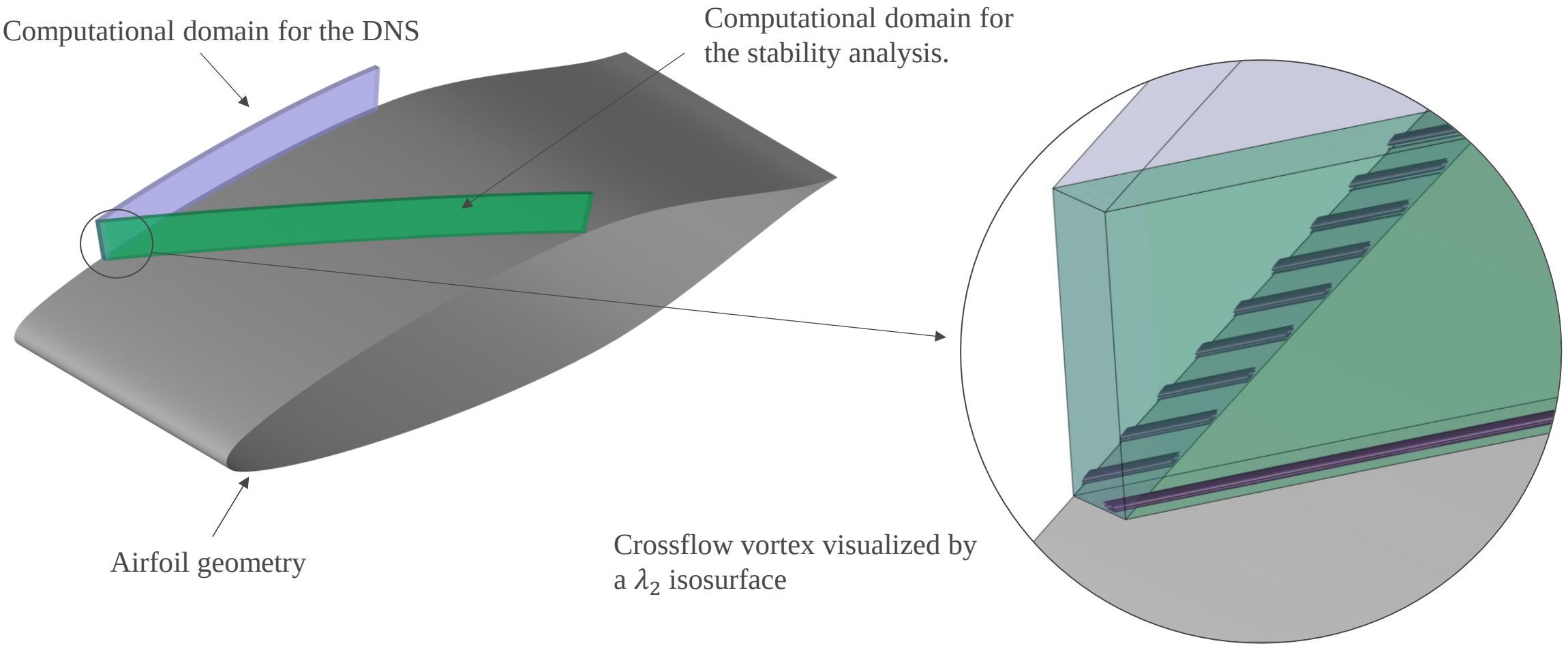


≈ 10² smaller out-of-plane derivatives

Aligning ξ with the minimum-variation direction strongly reduces the base flow variation normal to the marching planes.
→ **The base flow is therefore much closer to the slowly varying assumption used by the stability formulation.**

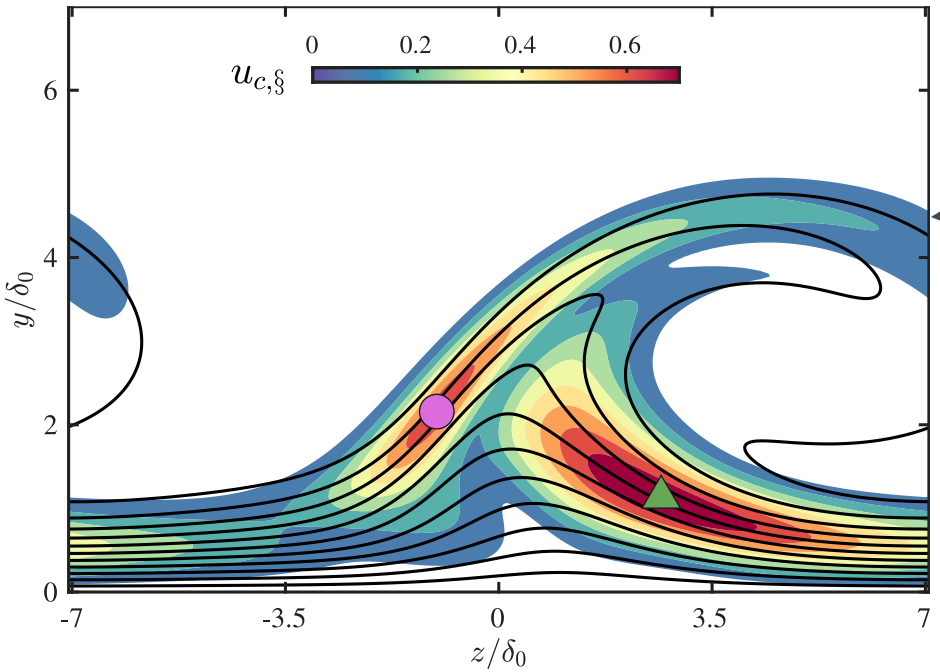
Three-dimensional computational domains

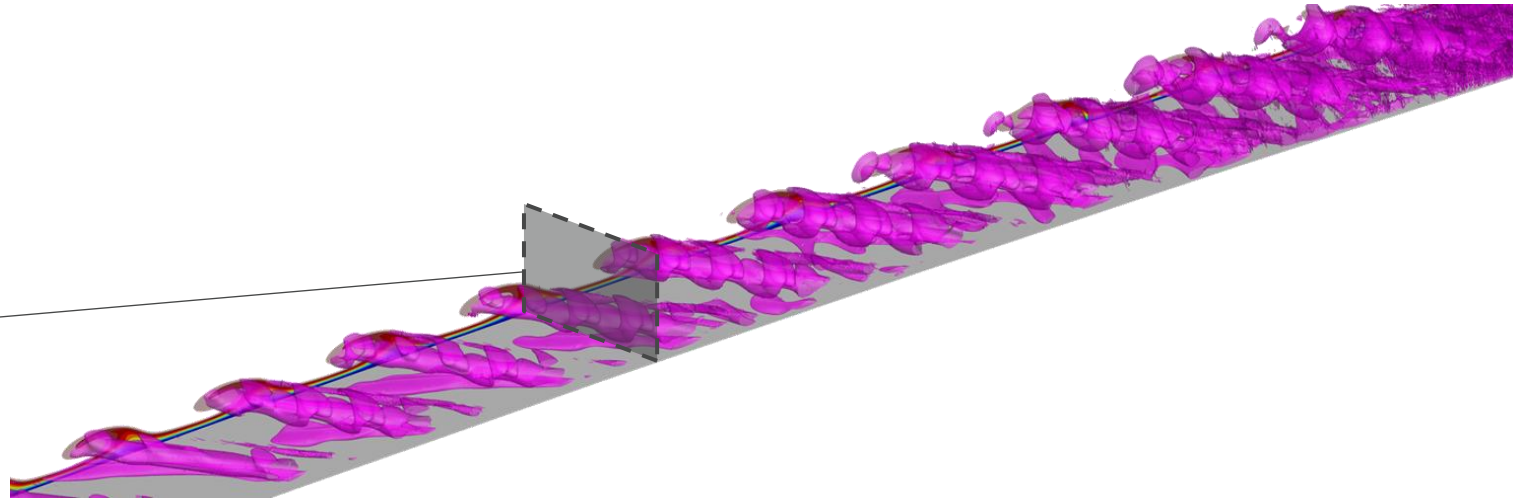
DNS reference domain and stability-analysis domain for the clean configuration



DNS spectral analysis

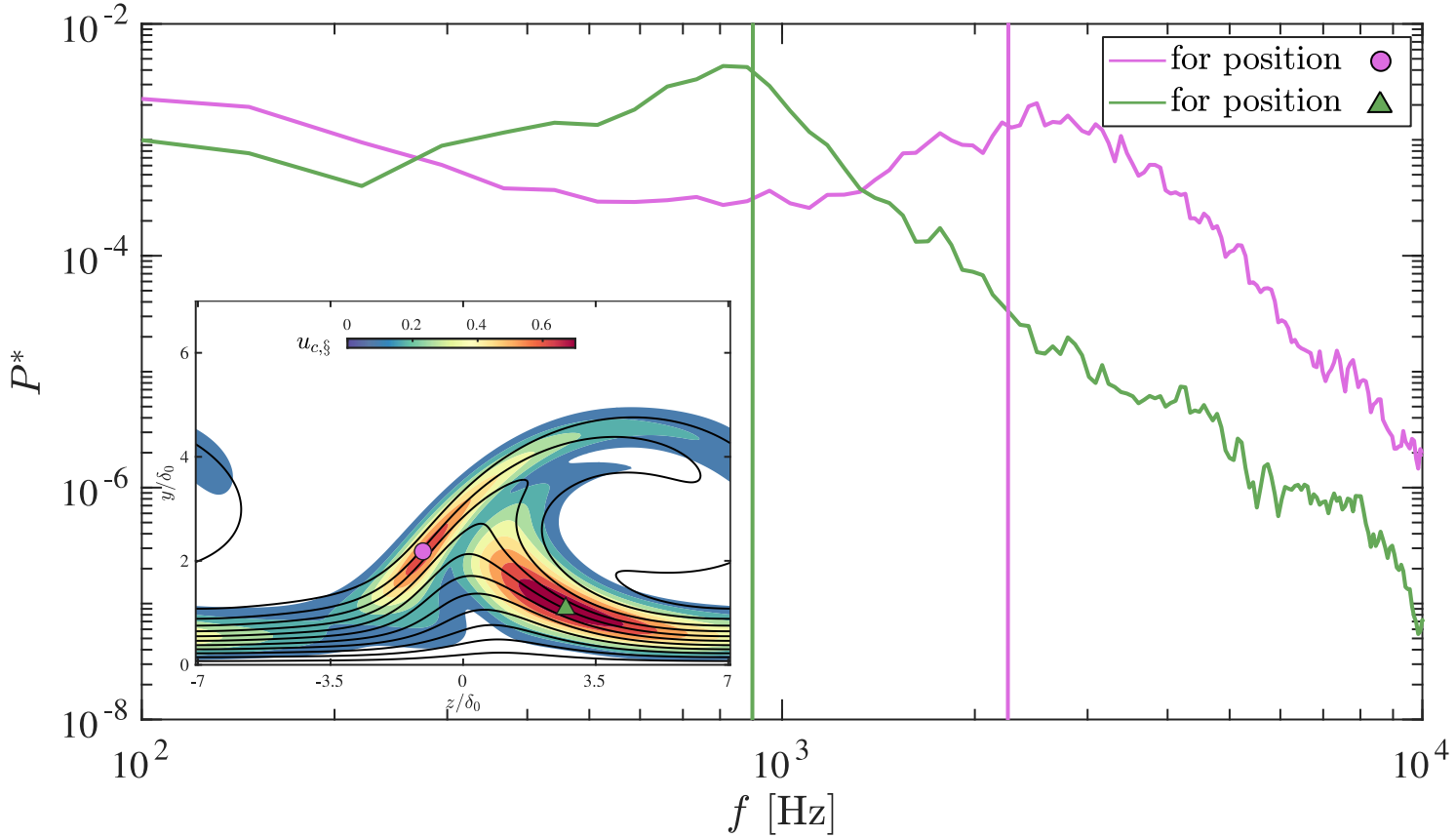
Identification of secondary-instability frequencies upstream of transition front





DNS spectral analysis

Identification of secondary-instability frequencies upstream of transition front



900 Hz **TYPE III**

Inner upwelling region

Pronounced low-frequency spectral energy associated with the inner fluctuation region.

2200 Hz **TYPE I**

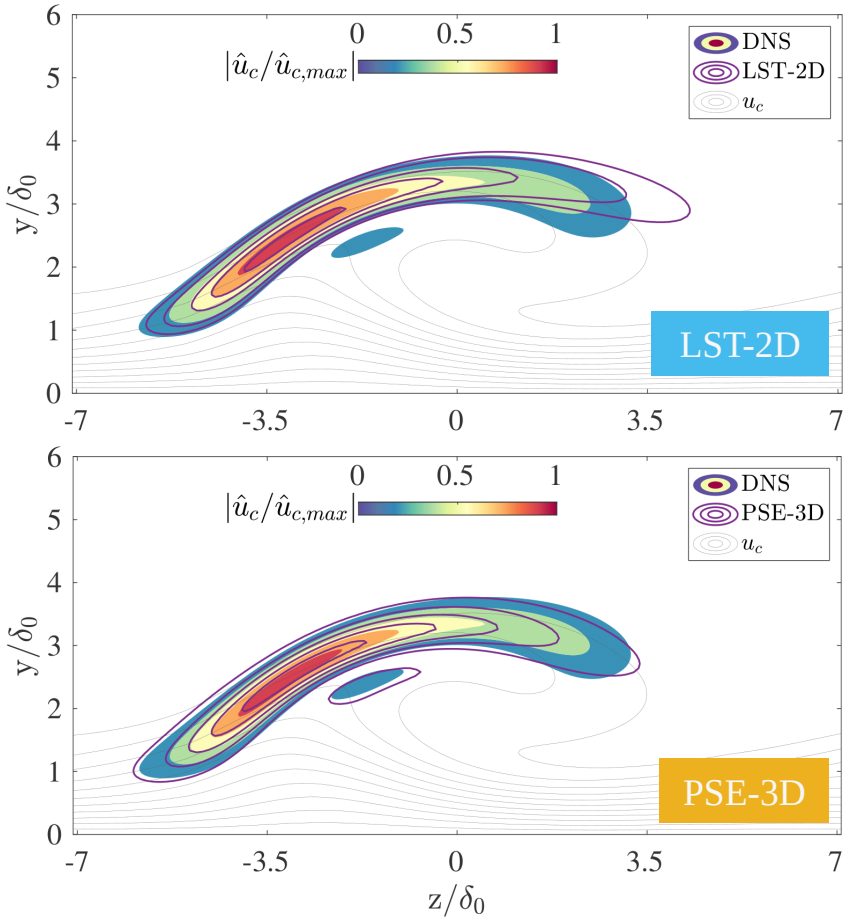
Outer upwelling region

Higher-frequency content representative of the outer secondary-instability region.

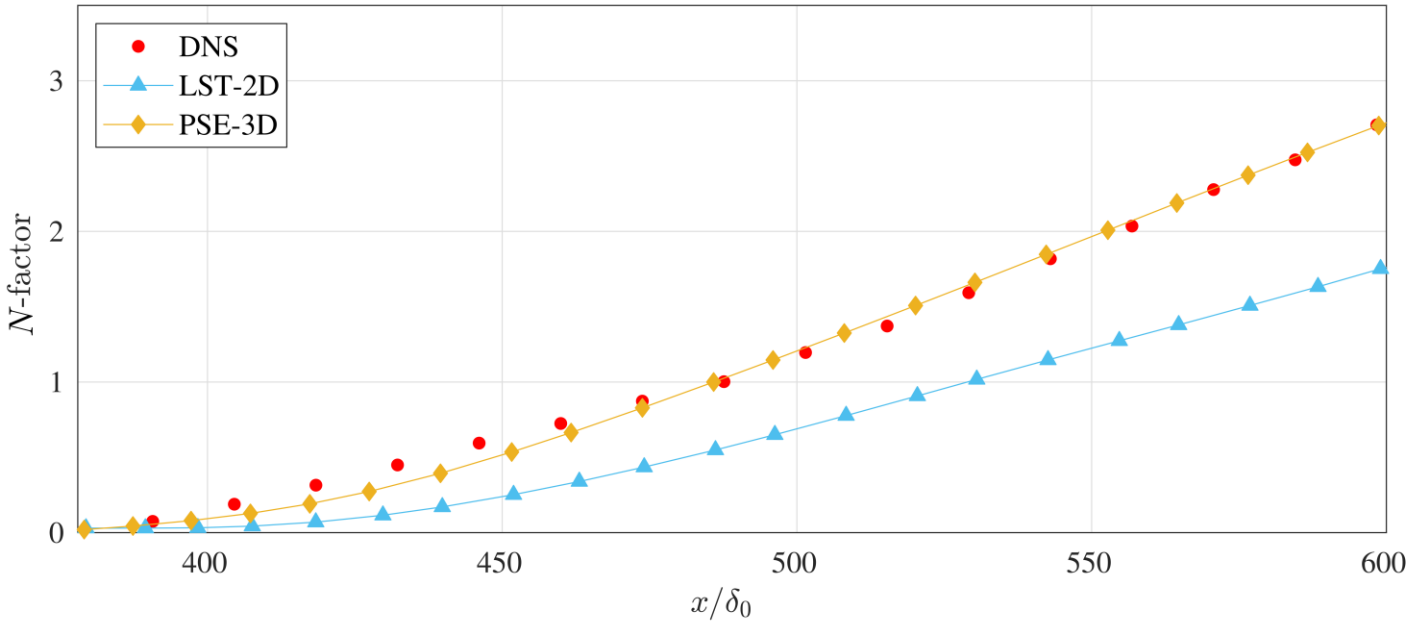
900 Hz (Type III) and 2200 Hz (Type I) are selected for LST-2D / PSE-3D comparison with DNS.

Type I secondary instability at 2200 Hz

DNS comparison with LST-2D and PSE-3D



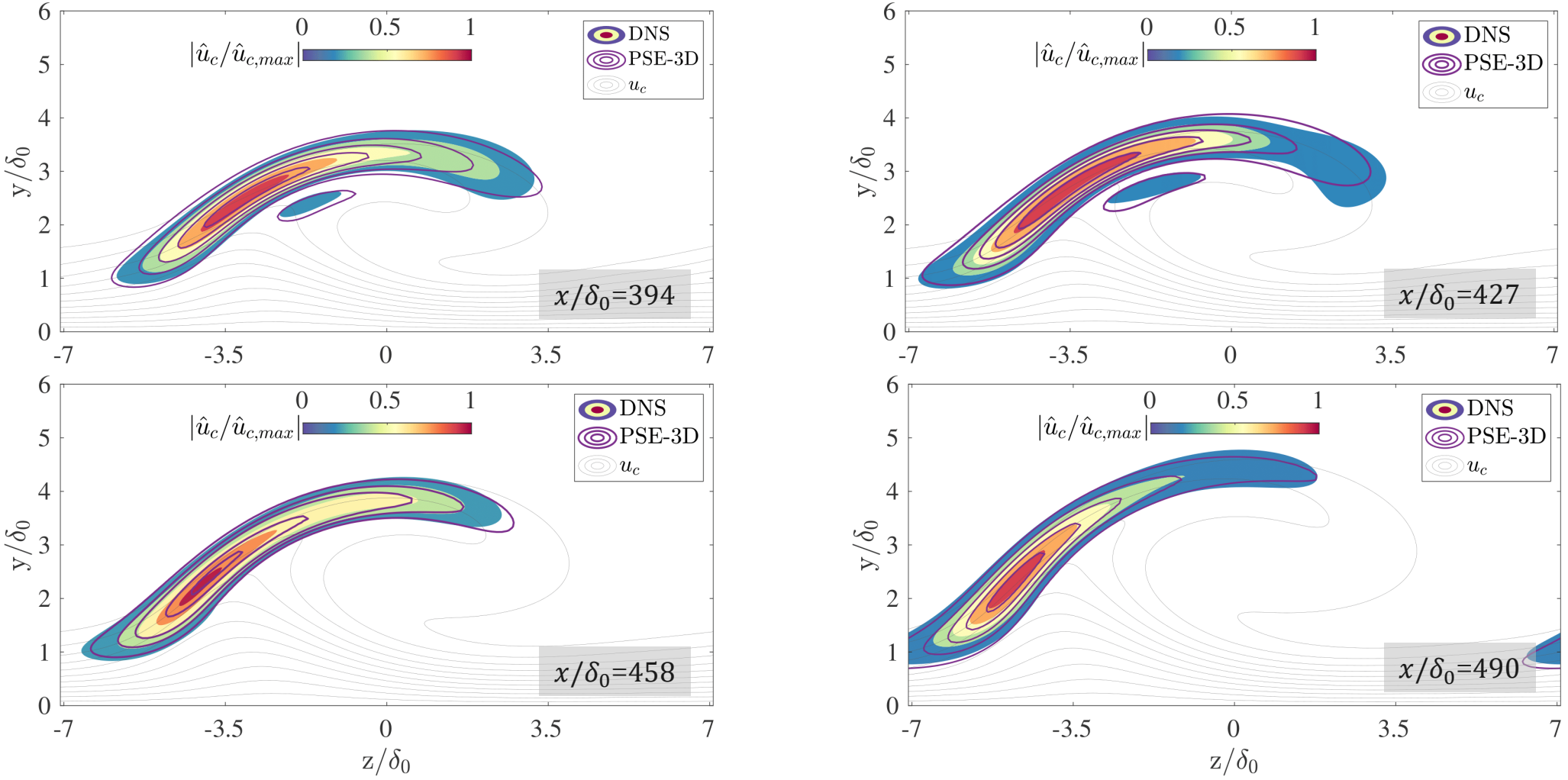
Normalized magnitude of the streamwise velocity component amplitude function ($|\hat{u}_c/\hat{u}_{c,max}|$)at $x/\delta_0 = 430$ (left). Integrated amplification factor curves versus x/δ_0 (right).



Both methods recover the Type I mode and PSE-3D provides the closest overall agreement with the DNS.

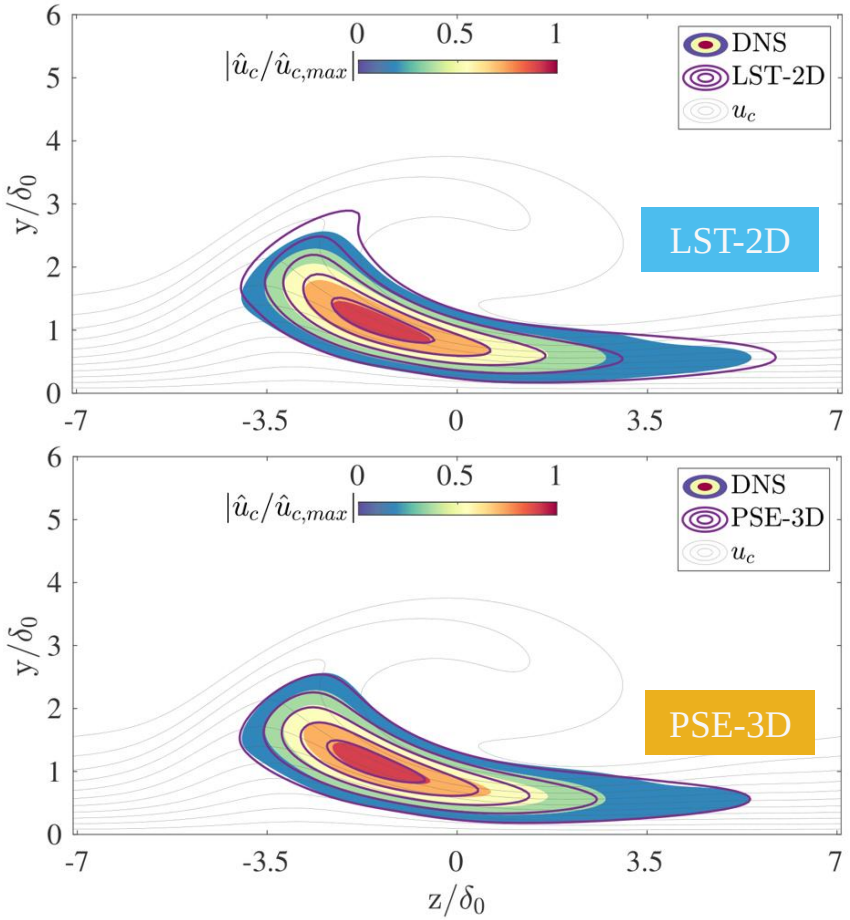
Streamwise evolution of the Type I at 2200 Hz

PSE-3D/DNS comparison

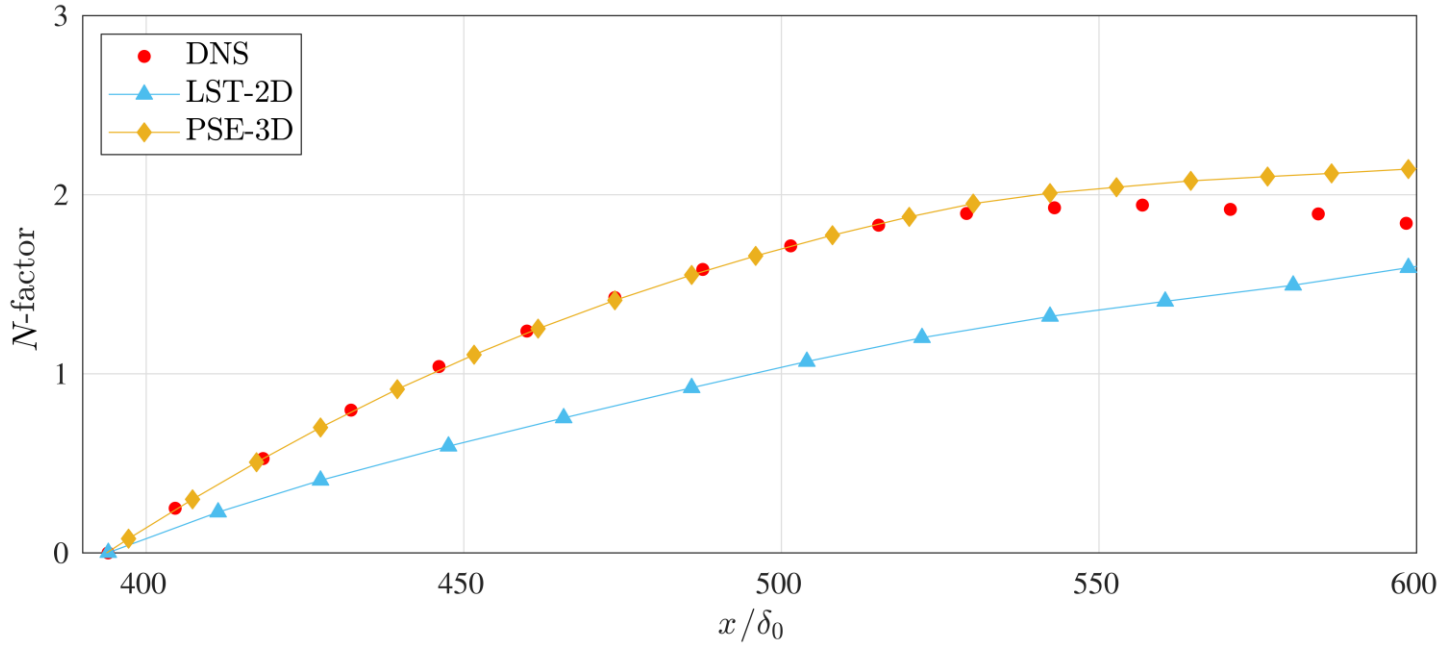


Type III secondary instability at 900 Hz

DNS comparison with LST-2D and PSE-3D



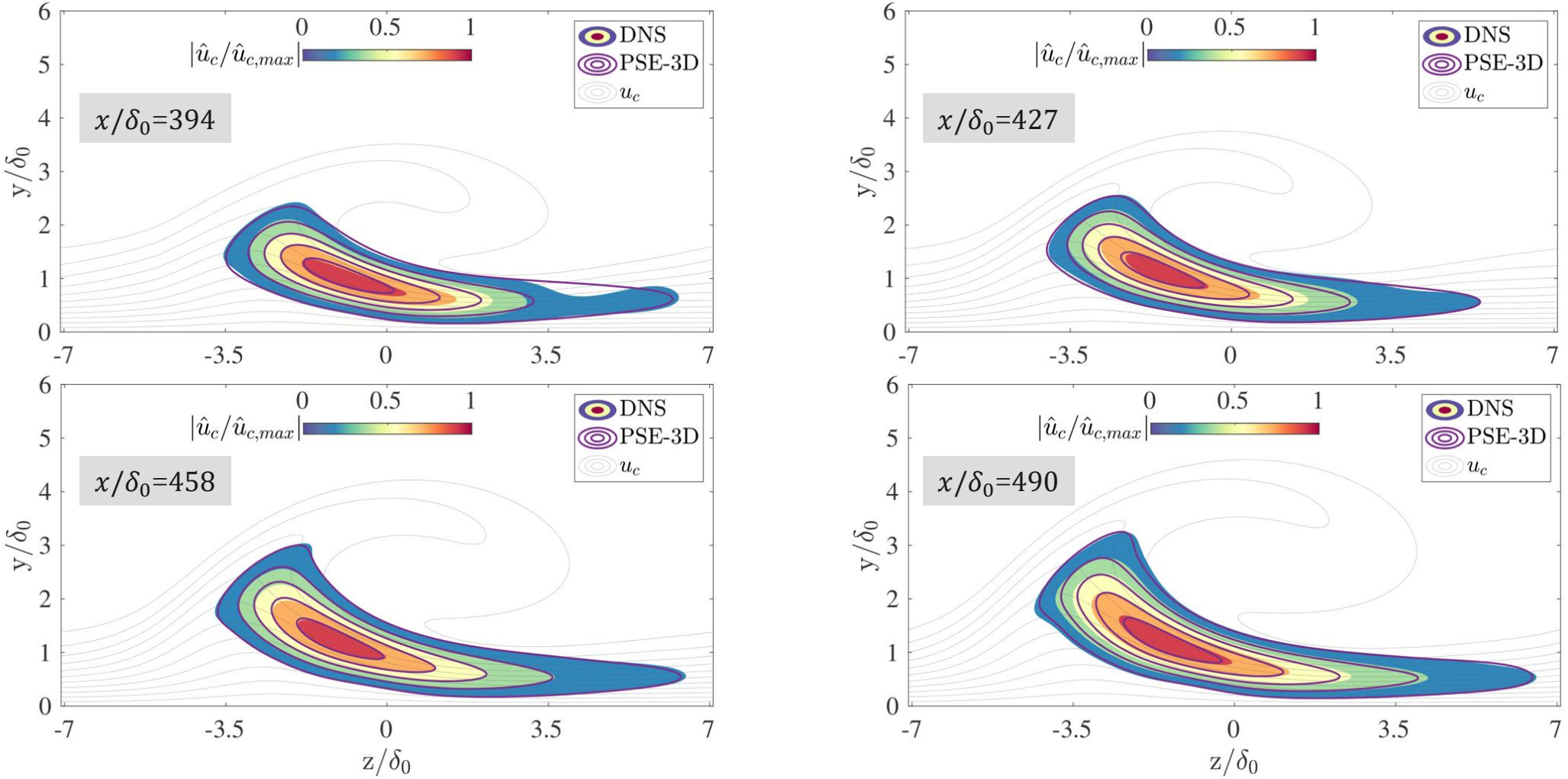
Normalized magnitude of the streamwise velocity component amplitude function ($|\hat{u}_c/\hat{u}_{c,max}|$)at $x/\delta_0 = 430$ (left). Integrated amplification factor curves versus x/δ_0 (right).



Both methods recover the Type III mode and PSE-3D provides the closest overall agreement with the DNS.

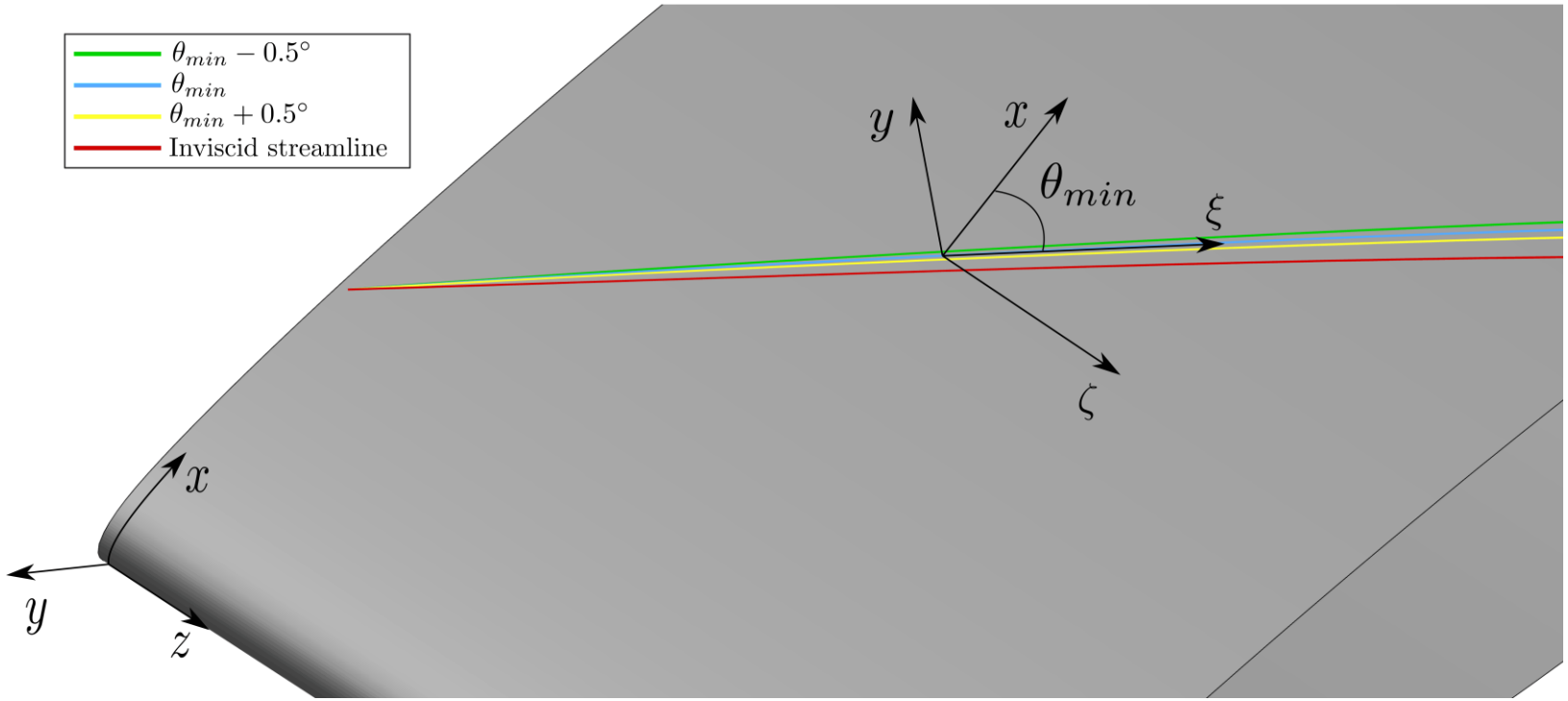
Streamwise evolution of the Type III at 900 Hz

PSE-3D/DNS comparison



Impact of coordinate-system orientation

Sensitivity of the predicted disturbance evolution to the out-of-plane direction



Reference direction

θ_{min} follows the minimum-variation direction and is used as the baseline integration path.

Perturbed directions

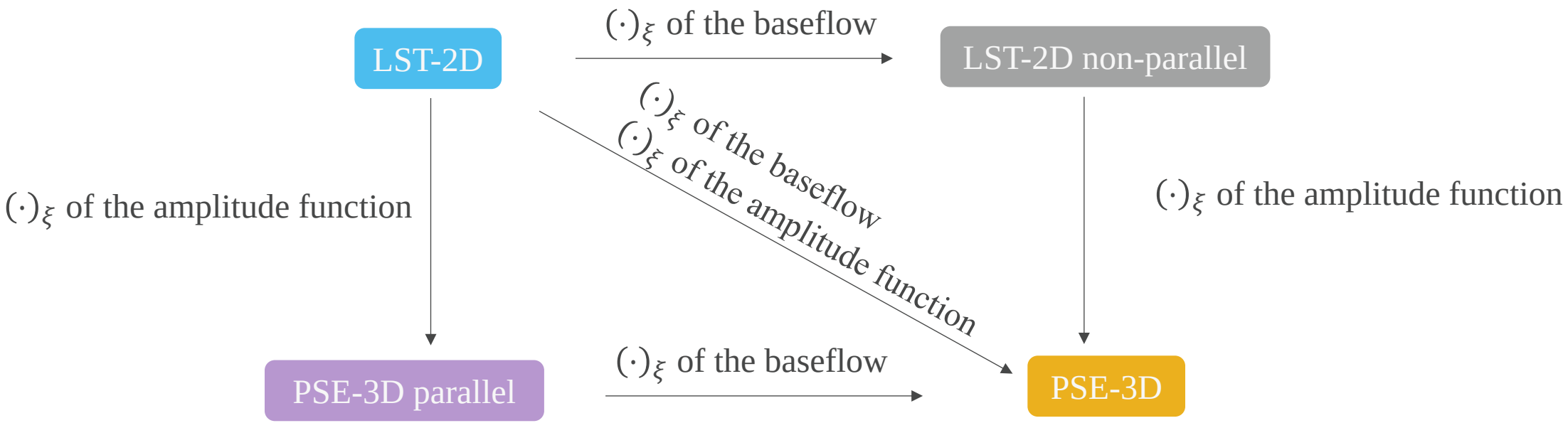
Small rotations around θ_{min} define different out-of-plane directions through the same base flow.

Resulting sensitivity

The predicted disturbance evolution changes appreciably when the integration direction is modified.

Intermediate stability formulations

Separating local/marching and parallel/non-parallel effects

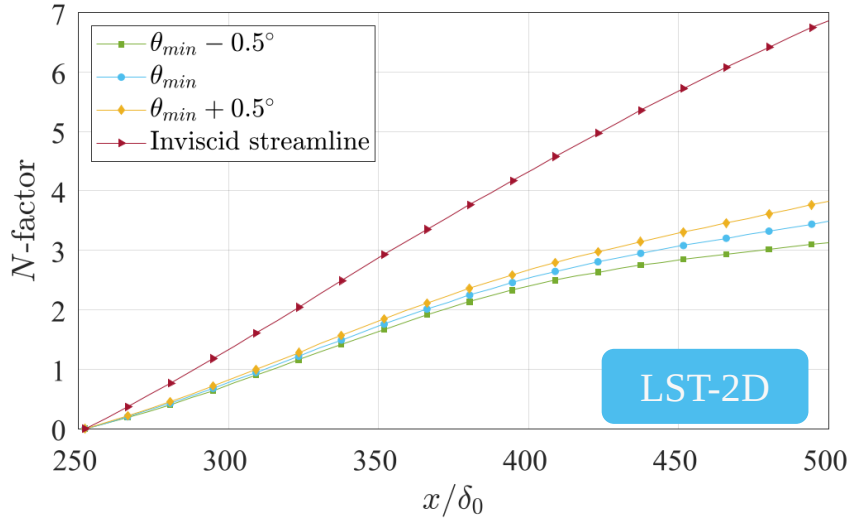


Intermediate methodologies considered to separate the *local/non-local* and *parallel/non-parallel* effects.

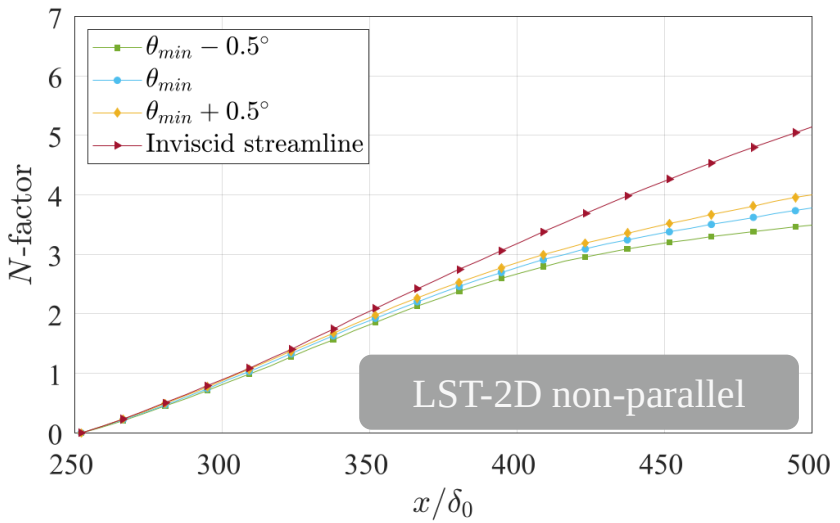
Comparison of intermediate formulations

Effect of intermediate assumptions on the predicted amplification

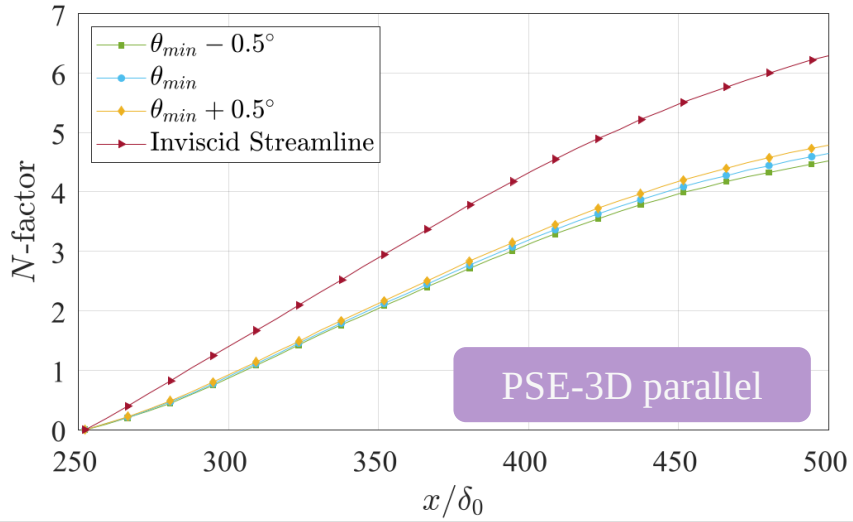
$(\cdot)_\xi$ of the amplitude function



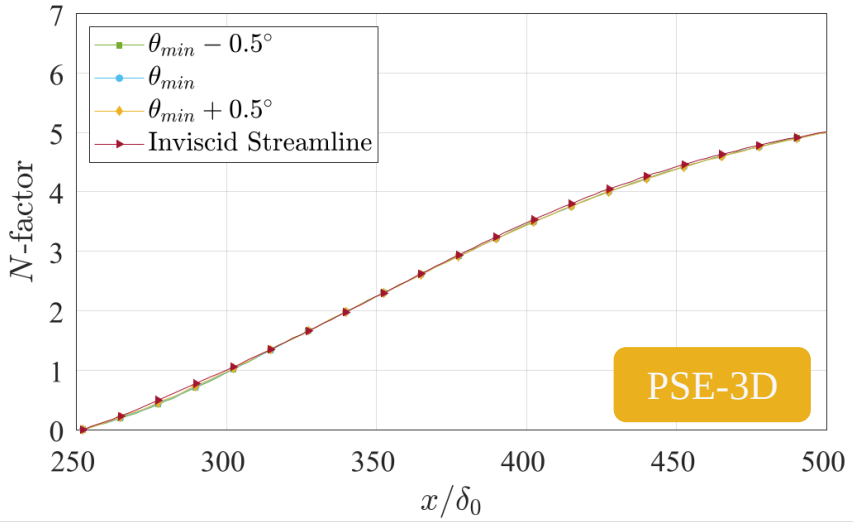
$(\cdot)_\xi$ of the baseflow



$(\cdot)_\xi$ of the amplitude function



$(\cdot)_\xi$ of the baseflow



From the clean configuration to smooth hump cases

Using the validated framework to investigate localized smooth surface deformations

CLEAN REFERENCE

Validated clean swept-wing reference

SMOOTH HUMP



Smooth, spanwise-homogeneous deformation with continuously varying slope and curvature.

Geometry

Defined by the hump height h, the widths σ_L and σ_R and the apex location x_h.

Physical effect

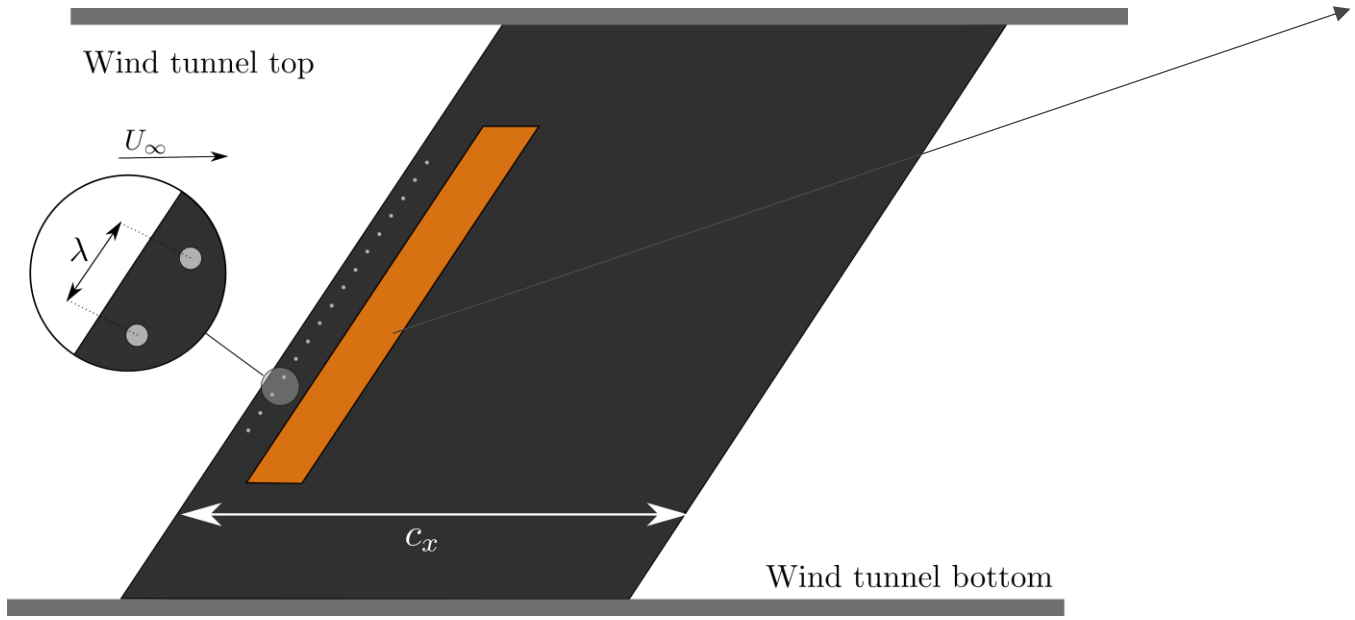
The hump modifies the local pressure-gradient and the development of the stationary crossflow vortex.

Question addressed

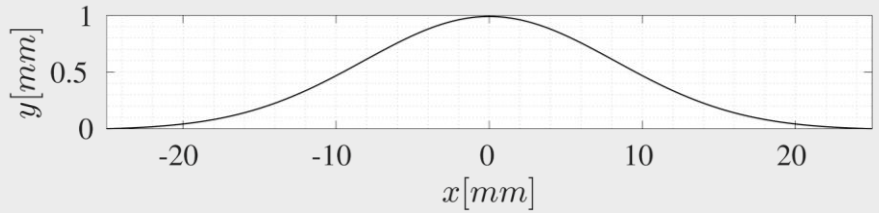
How do smooth humps alter the secondary-instabilities and the transition scenario relative to the clean reference?

Smooth-hump configuration

Reference hump and incoming stationary-crossflow amplitude levels



REFERENCE HUMP GEOMETRY



Smooth, spanwise-homogeneous surface deformation with continuously varying slope and curvature.

Case	h [mm]	Amplitude	DREs x/c
C_{0,A_1}	0	A_1	0.05
H_{0,A_1}	1	A_1	0.05
C_{0,A_2}	0	A_2	0.02
H_{0,A_2}	1	A_2	0.02

Based on the TU Delft swept-wing experiment.

Vidales & Kotsonis, JFM 1014:A35 (2025)

Experimental observations with the reference hump

Hump-dependency on amplitude of incoming stationary crossflow

A_1

CLEAN	H_0	OUTCOME
Type-I route	Smooth hump	Transition delay

For the low-amplitude case, the hump acts as a stabilising device and shifts transition downstream.

H_0 is beneficial in A_1

A_2

CLEAN	H_0	OUTCOME
Type-I route	Smooth hump	Earlier transition

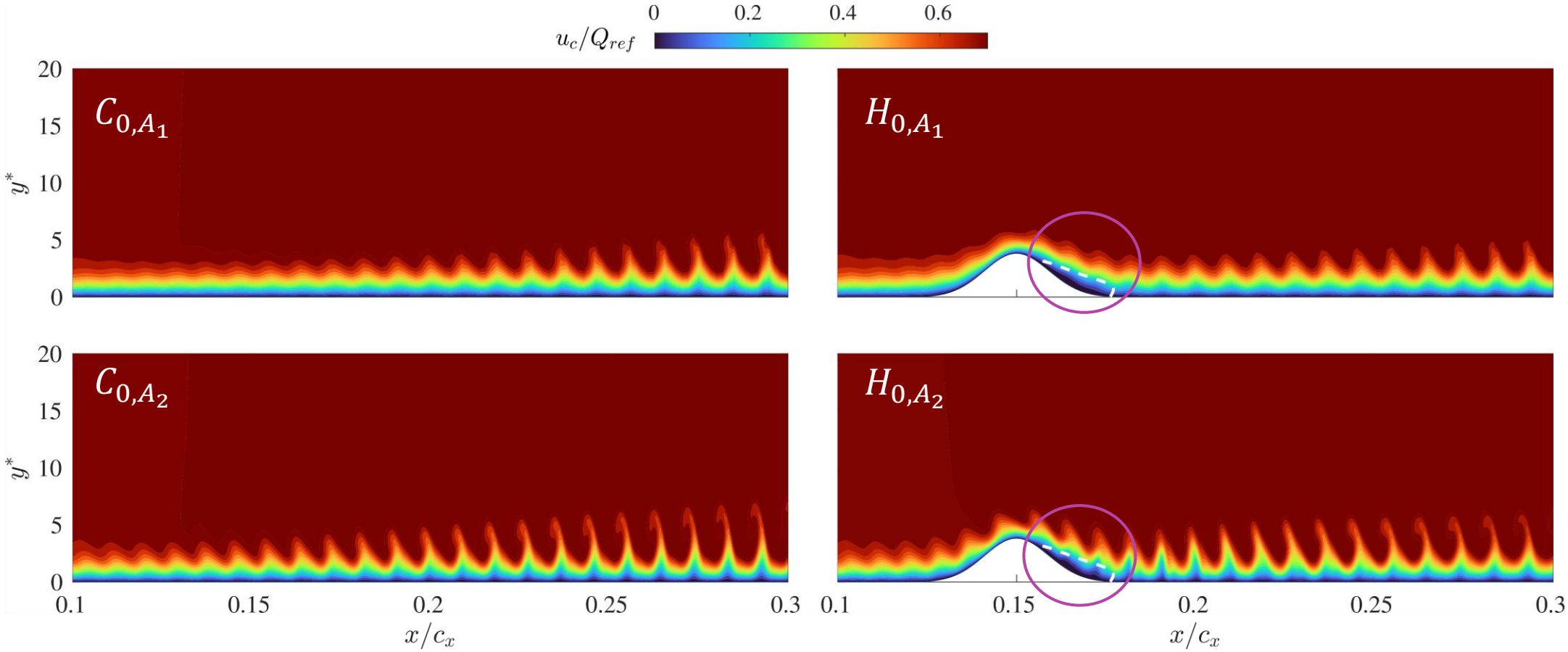
For the high-amplitude case, the same hump no longer delays transition and may even promote an earlier breakdown.

H_0 is not universally stabilising

The effect of the reference hump depends on the amplitude of the incoming stationary vortex.

Base-flow distortion induced by the smooth hump

Streamwise velocity field and crossflow-reversal region in the chordwise plane

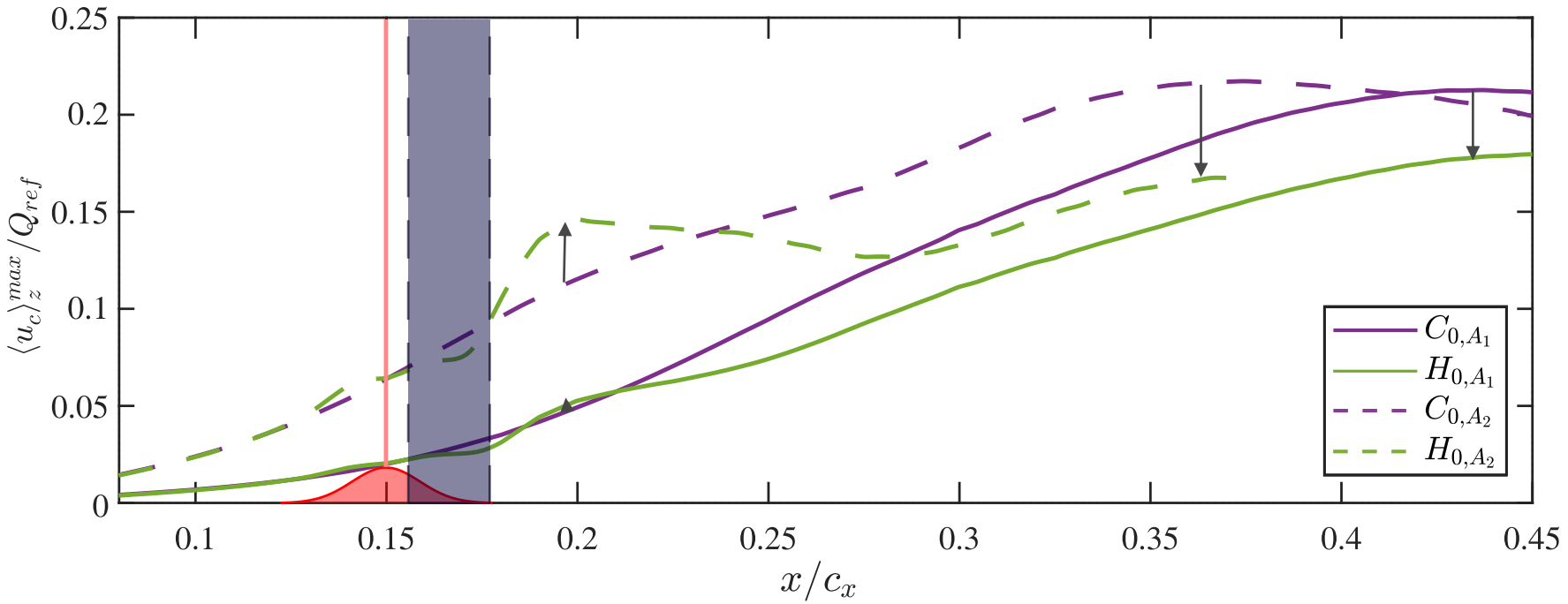


The smooth hump locally reorganizes the stationary crossflow-vortex, inducing crossflow reversal

Data note: the DNS database used in this work was developed in collaboration with Mohammad Moniripiri (KTH Stockholm).

Effect of the smooth hump on primary crossflow growth

Wall-normal maximum of the spanwise standard deviation of the chordwise velocity



Near-hump response

Approaching the hump and up to $x/c_x \approx 0.2$, both H_{0,A_1} and H_{0,A_2} exceed the corresponding clean cases.

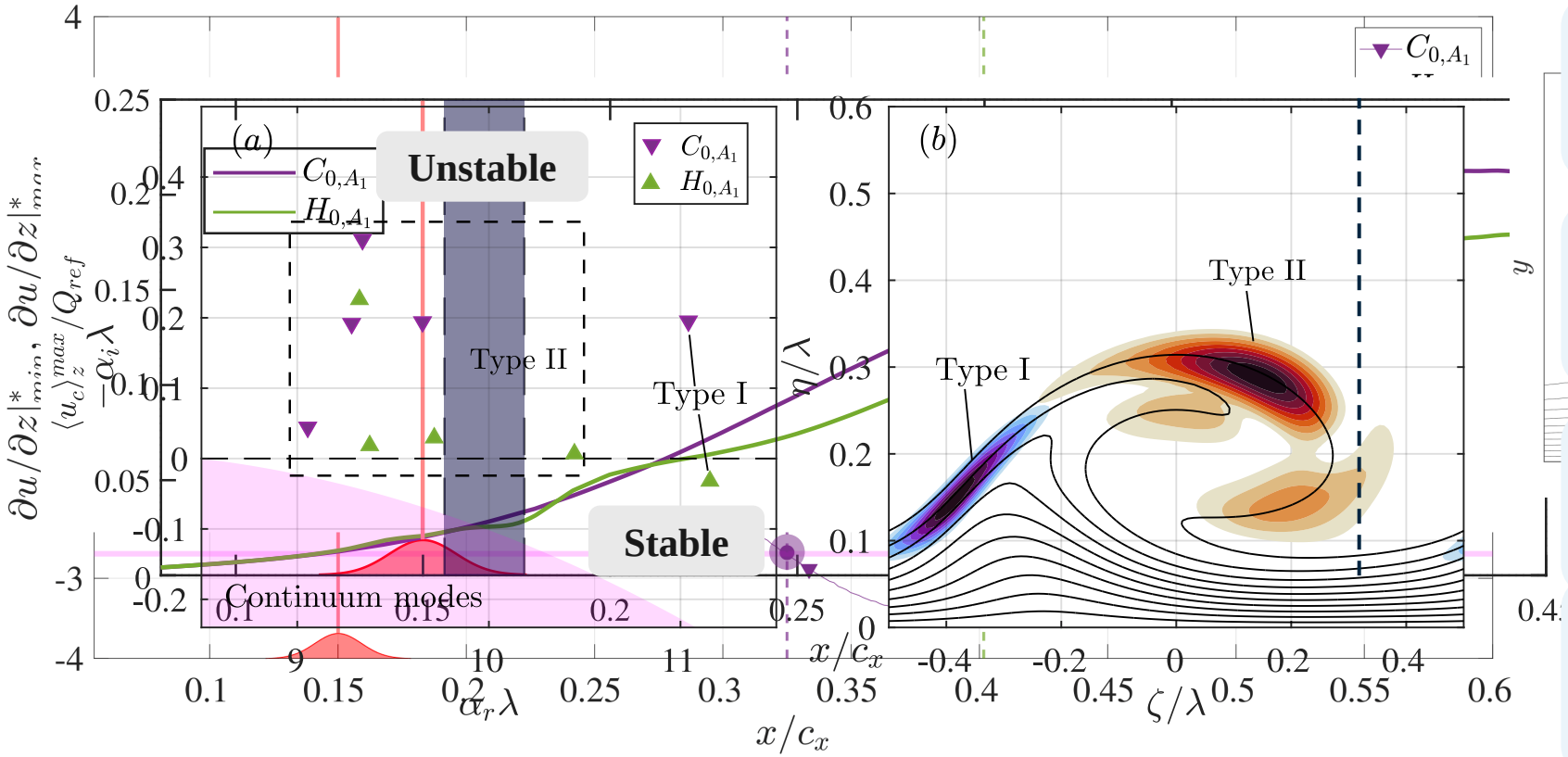
Downstream effect

For $x/c_x > 0.2$, both hump cases show a strong stabilisation trend of the stationary CF amplitude.

The hump destabilizes the stationary CF mode locally, but stabilizes it downstream.

High-frequency secondary instabilities in the low-amplitude hump case

Influence of the smooth hump on the classical Type I/II: eigenvalue spectra at 5000 Hz



Shared modes weakened
Modes also present in the clean case are significantly weaker in H_{0,A_1}.

Type I suppressed
Type I becomes stable in the hump case at the considered station and frequency.

Negligible *N*-factors
High-frequency amplification is limited and yields negligible *N*-factor growth.

Cause
Weakening of the stationary vortex and therefore of the shear layers supporting the classical secondary instabilities.

In the low-amplitude case, the smooth hump suppresses the classical high-frequency secondary-instability route.

High-amplitude hump case: why is transition not delayed?

The classical high-frequency secondary-instability route is also damped

LOW-AMPLITUDE HUMP CASE

H_{0,A_1}

Classical Type I/II modes weakened

→ **transition is delayed**

same trend?

HIGH-AMPLITUDE HUMP CASE

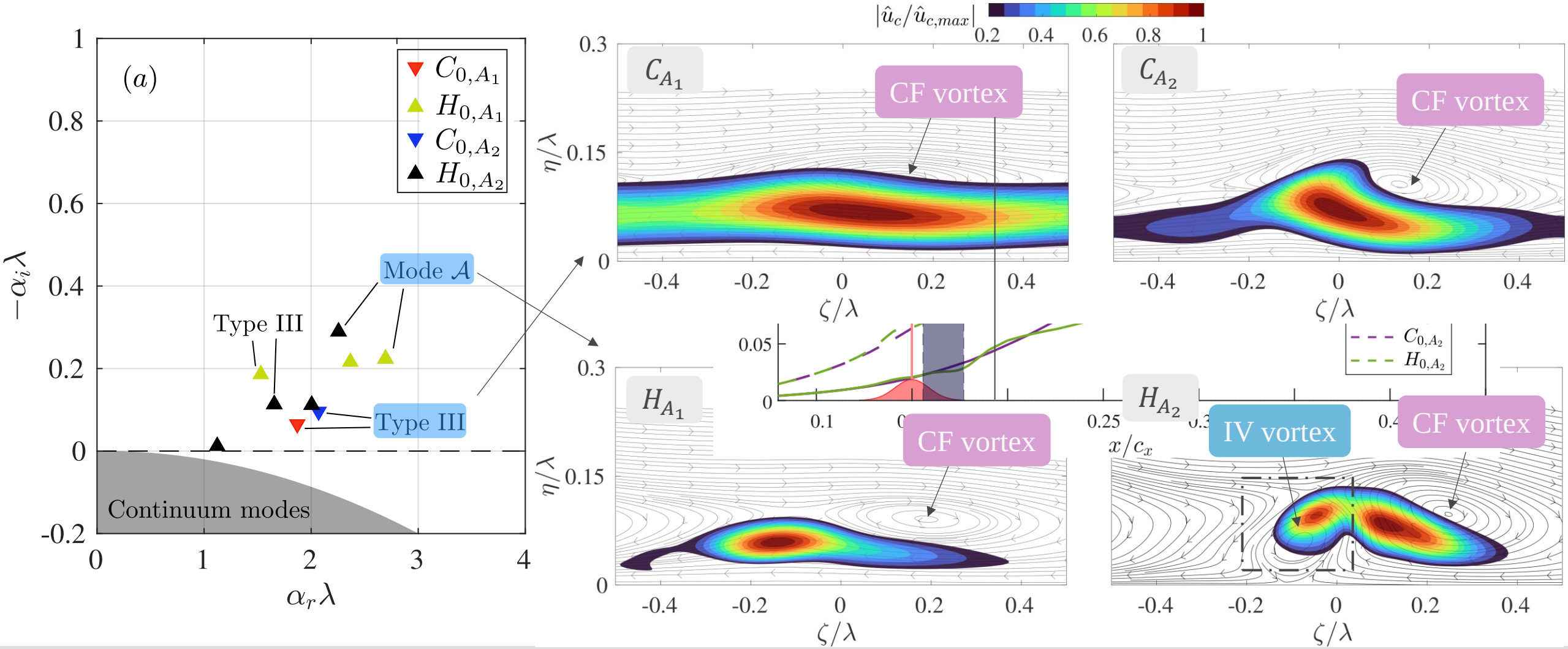
H_{0,A_2}

Classical Type I/II modes also weakened

→ **but transition is not delayed**

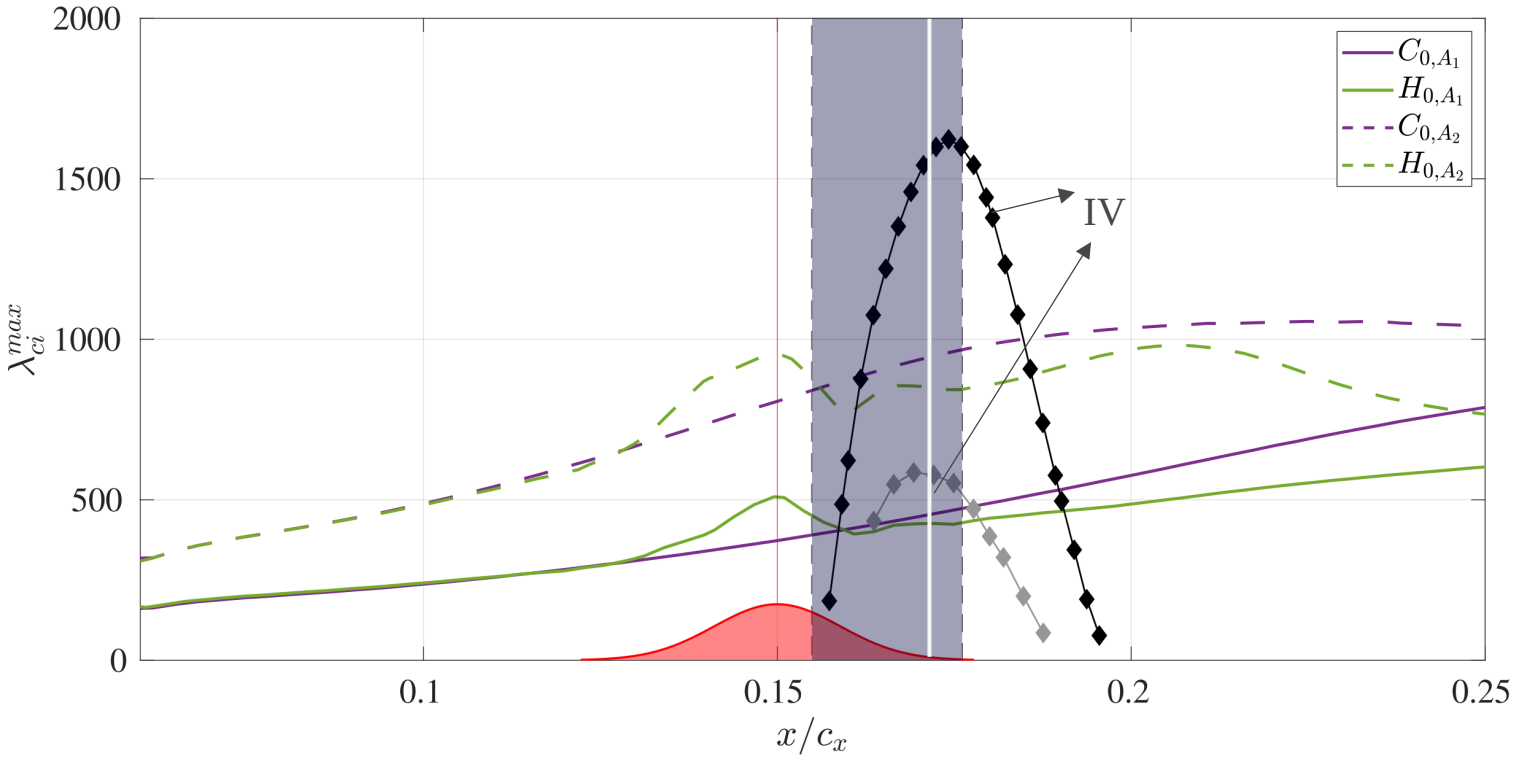
Hump-induced low-frequency Mode $\mathcal{A}$

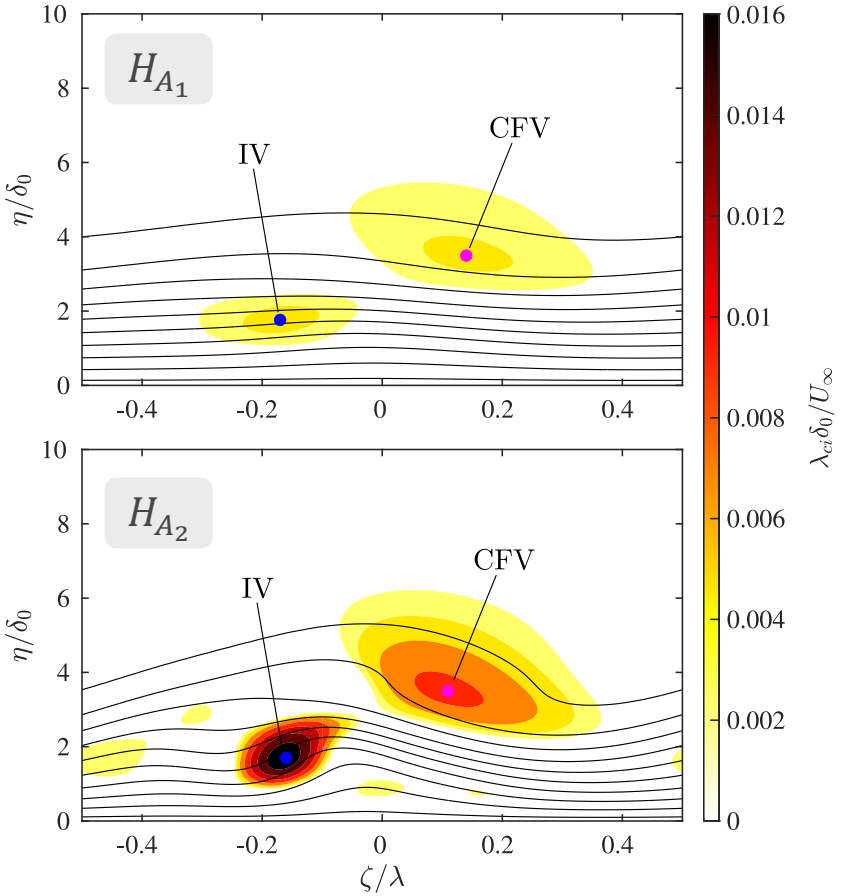
Influence of the smooth hump on the low-frequency instabilities: eigenvalue spectra at 500 Hz



Vortex identification using swirling strength

Quantifying the hump-induced vortex system through the local swirling angular frequency λ_{ci}

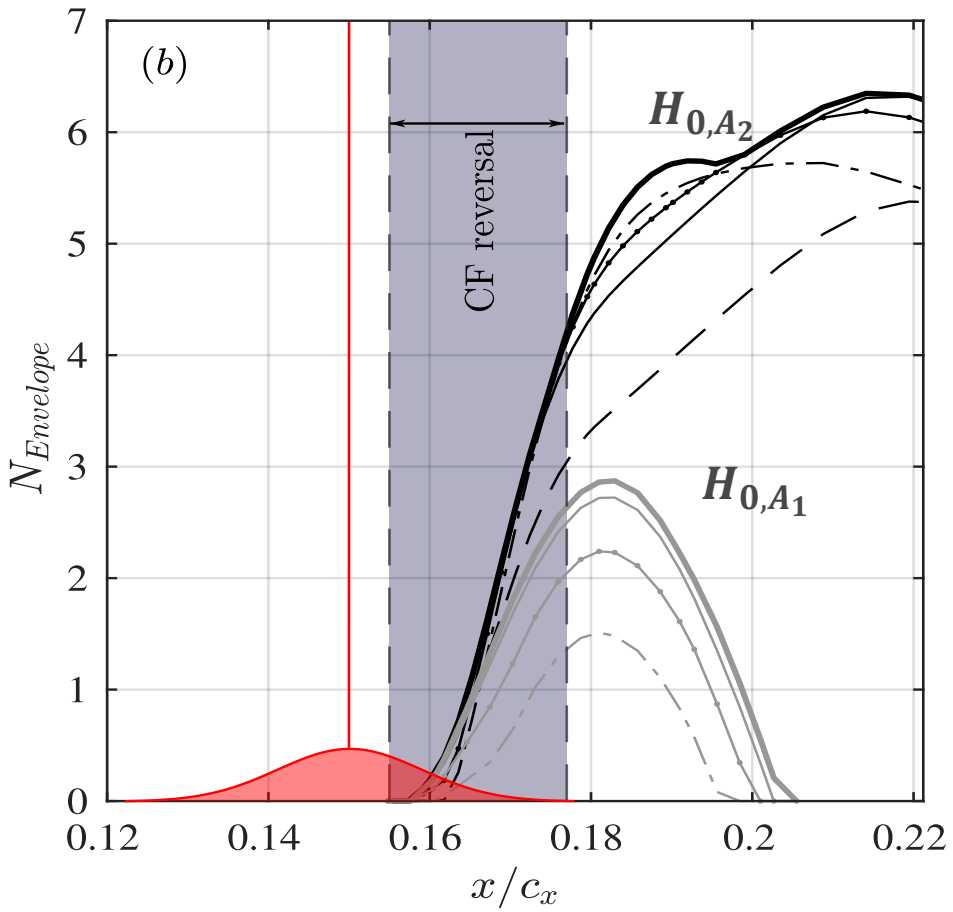




The high-amplitude case develops a much stronger and longer-living hump-induced vortex.

Amplification of the hump-induced Mode $\mathcal{A}$

Low-frequency branch reaches transition-relevant *N*-factors in the high-amplitude hump case



N-factors

Mode $\mathcal{A}$ is more unstable in the *high*-amplitude case (black lines) compared to the *low*-amplitude case (grey lines), reaching very large *N*-factors

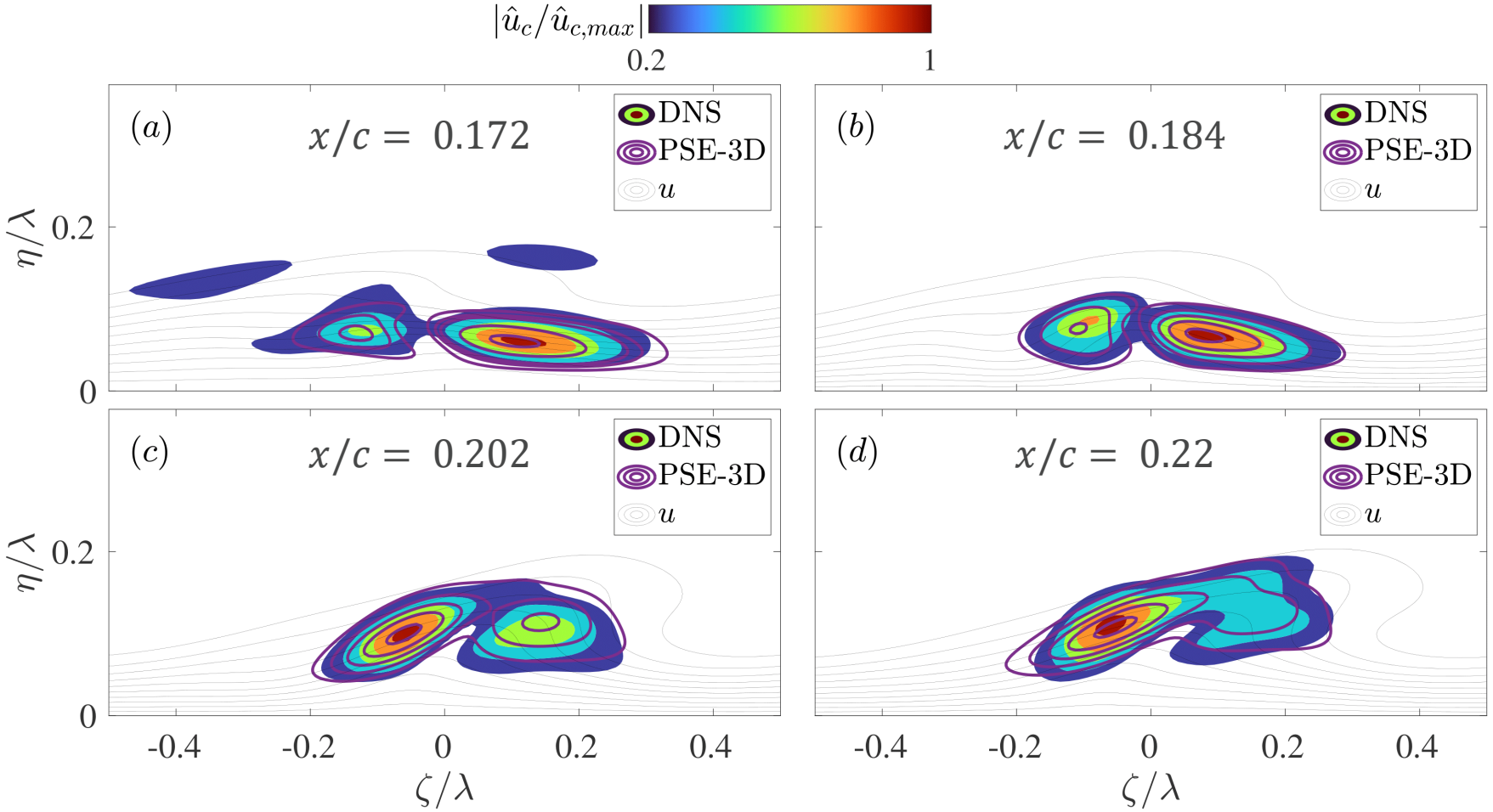
Convective instability

The large amplification of this perturbation indicates that this strong convective instability could be responsible for the different transition scenario in H_{A_2}

Mode $\mathcal{A}$ grows rapidly through the CF-reversal region, triggering transition in the H_{0,A_2} case.

Spatial structure of the hump-induced Mode $\mathcal{A}$ at 1200 Hz

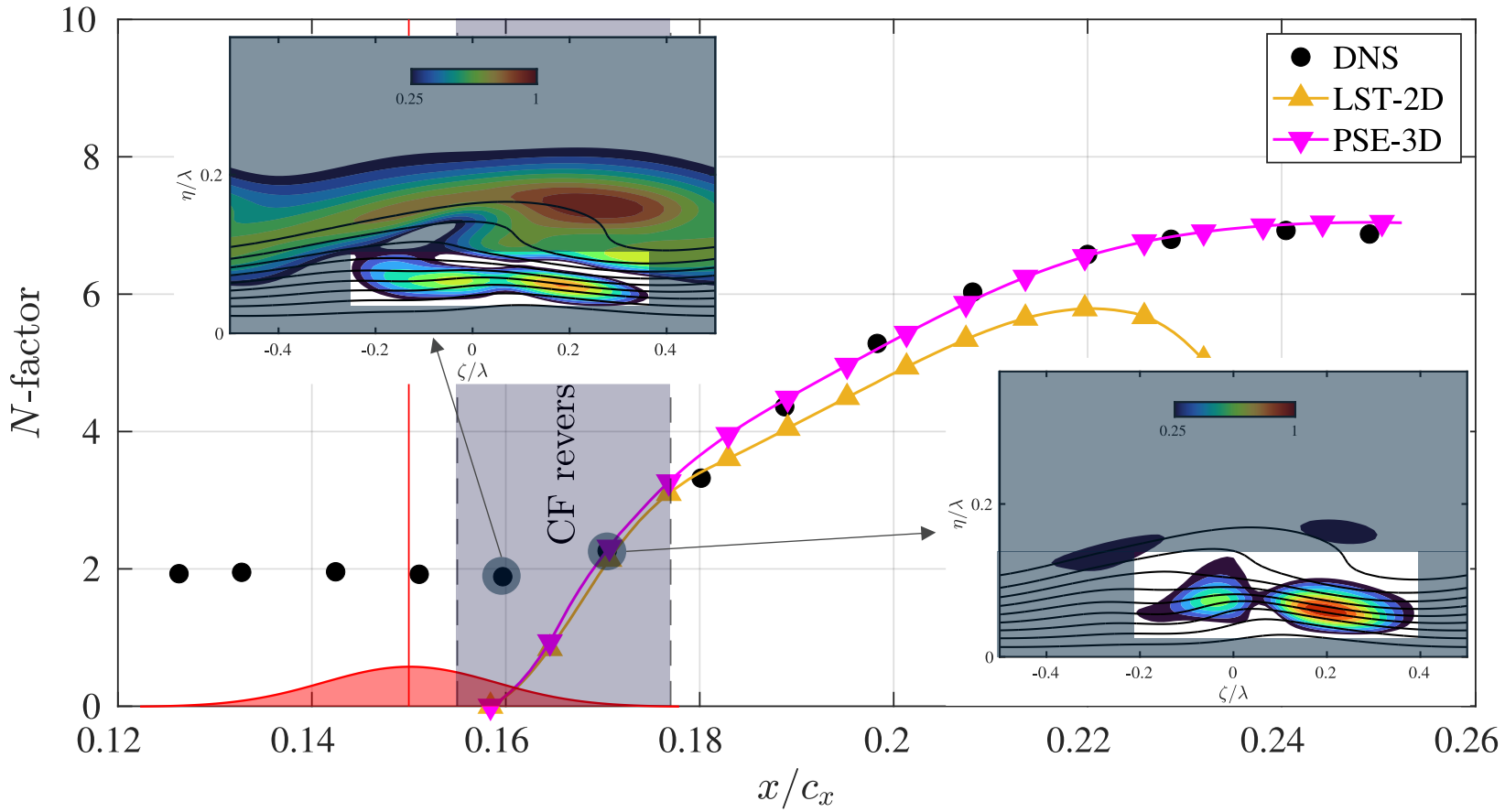
PSE-3D/DNS comparison at the peak-frequency in the high-amplitude hump case



PSE-3D reproduces the spatial structure of the low-frequency Mode A observed in DNS.

DNS validation of the Mode $\mathcal{A}$ amplification

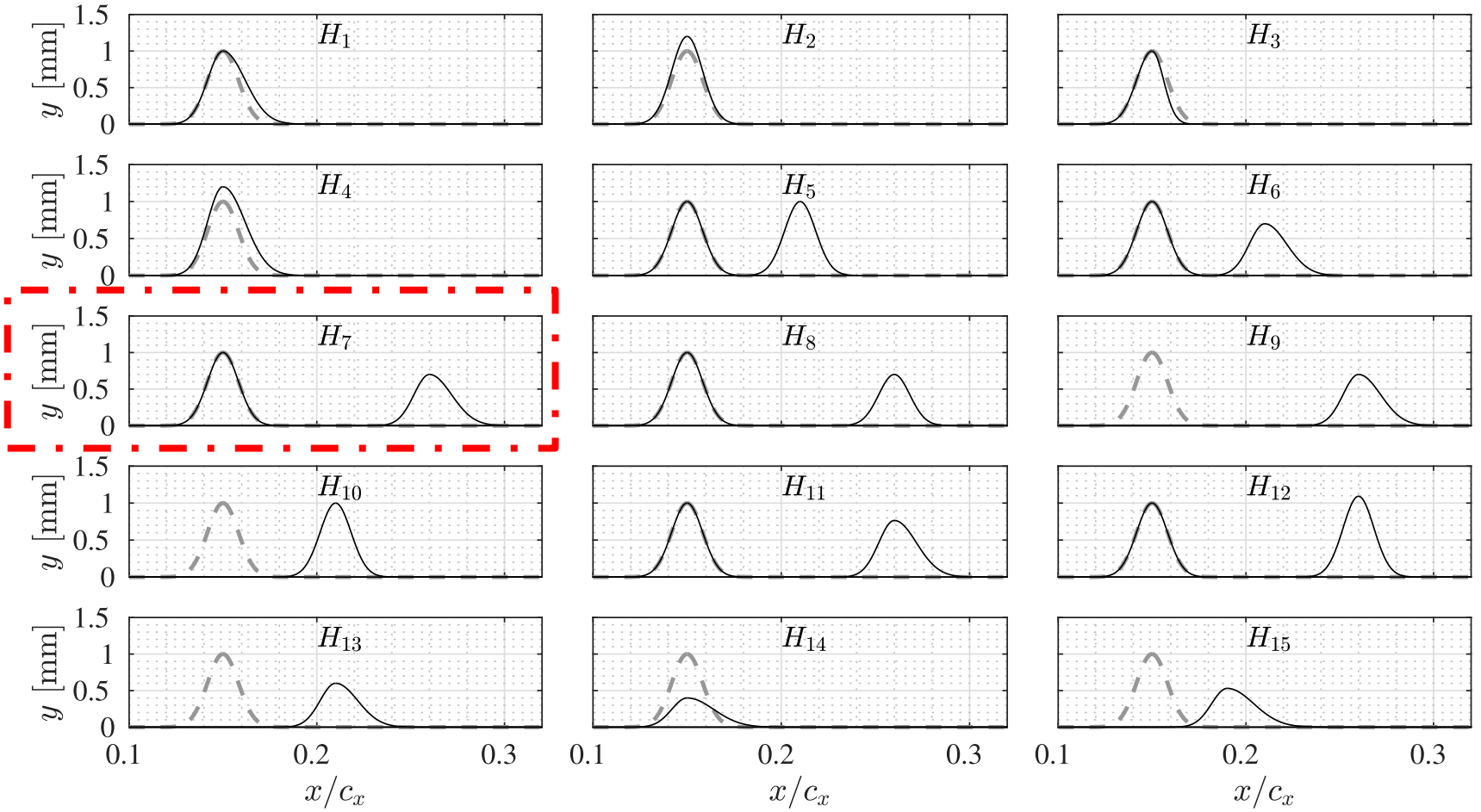
Comparison PSE-3D/DNS for the integrated growth rate



PSE-3D results on Mode $\mathcal{A}$ agree with DNS, confirming its convective nature and supporting it as the transition-relevant mechanism in H_{0,A_2}.

Parametric hump study: geometries considered

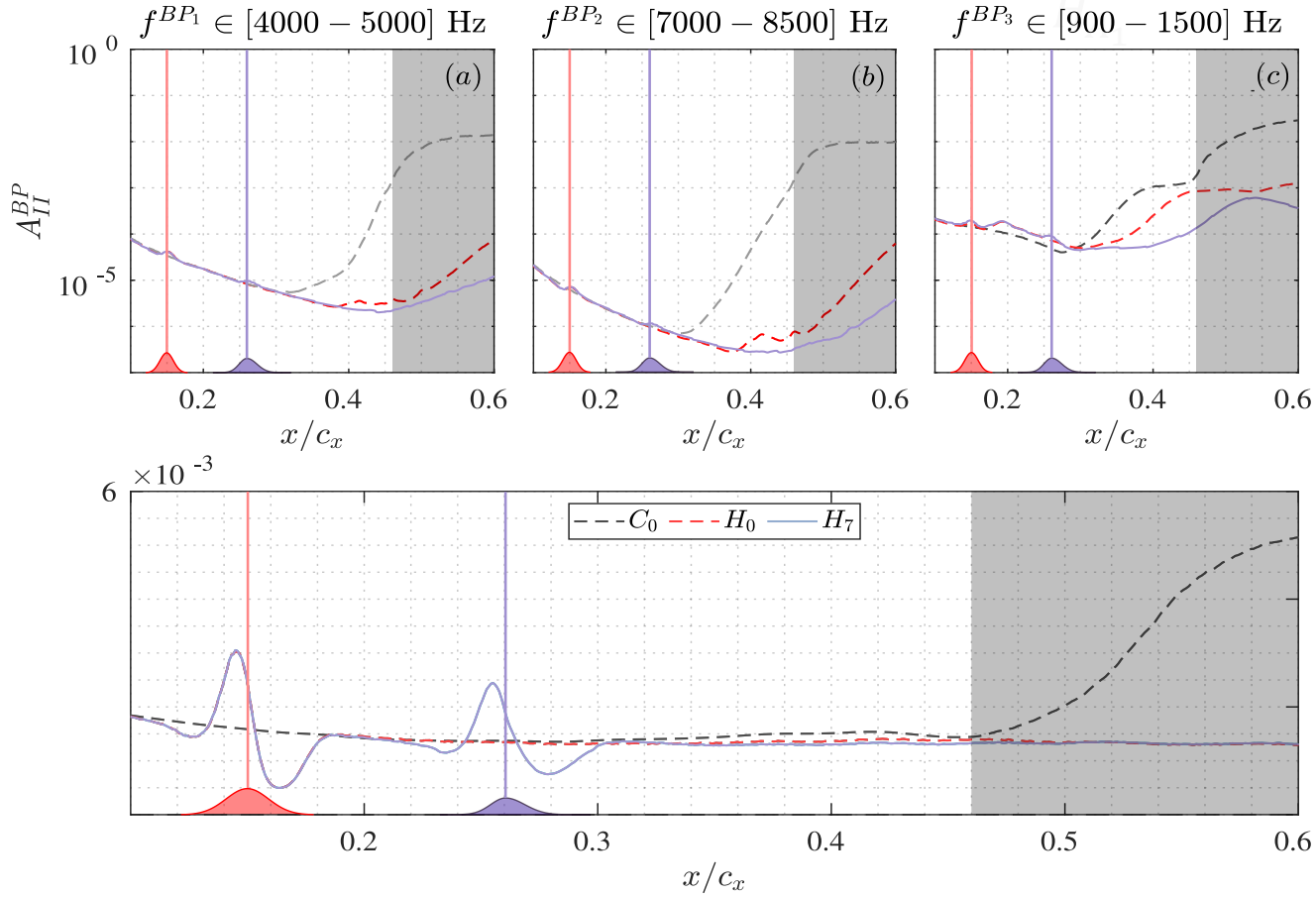
Single- and double-hump configurations used to test stabilisation strategies



The parametric study aimed for hump geometries that stabilise the stationary crossflow vortex.

Unsteady DNS of the double-hump case H7

Band-pass (BP) filtered disturbances confirm delayed amplification of secondary instabilities



BP1 / BP2
High-frequency secondary modes start amplifying farther downstream in H_7.

NEUTRAL POINTS
Shifted to $x/c_x \approx 0.45$ in H_7, compared with ≈ 0.39 for H_0.

SKIN FRICTION
C_0 transitions near $x/c_x \approx 0.46$. H_0 and H_7 remain laminar in the DNS domain.

H_7 pushes the onset of high-frequency secondary-instability amplification downstream compared to H_0

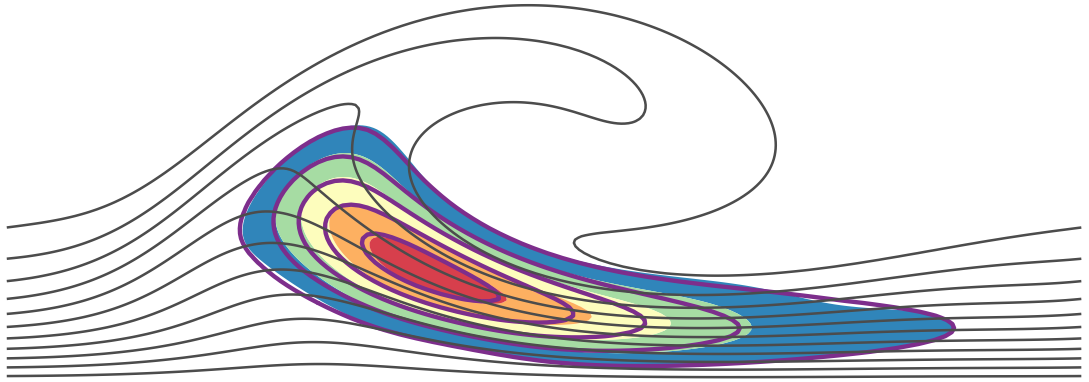
Conclusions

Key outcomes from the stability analysis of swept-wing boundary layers with surface irregularities

1 **Predictive framework**

Curvilinear non-orthogonal coordinates align ξ with the least-varying base-flow direction and preserve ζ-periodicity.

PSE-3D accurately reproduces the perturbation evolution and mode shape; LST-2D tends to under-predict growth.



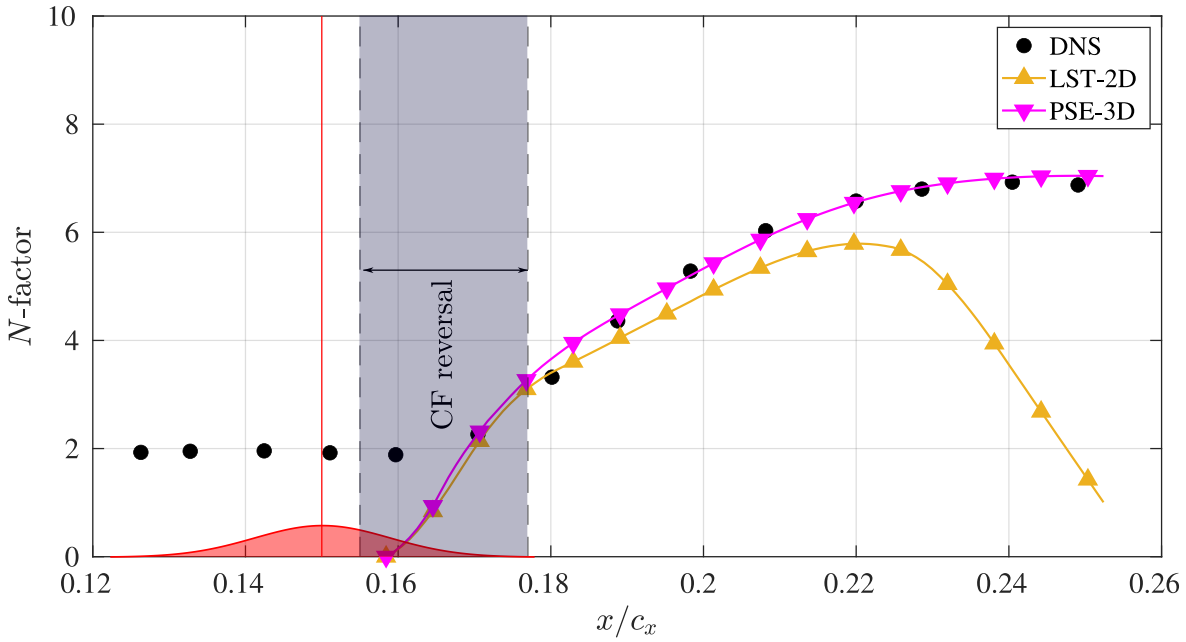
Conclusions

Key outcomes from the stability analysis of swept-wing boundary layers with surface irregularities

2 **Applicability to surface irregularities**

Steps and smooth humps strongly distort the base flow and generate crossflow-reversal regions with steep shear.

Despite this complexity, PSE-3D reproduces DNS mode shapes and *N*-factor evolution for the dominant instability.



1 **Predictive framework**

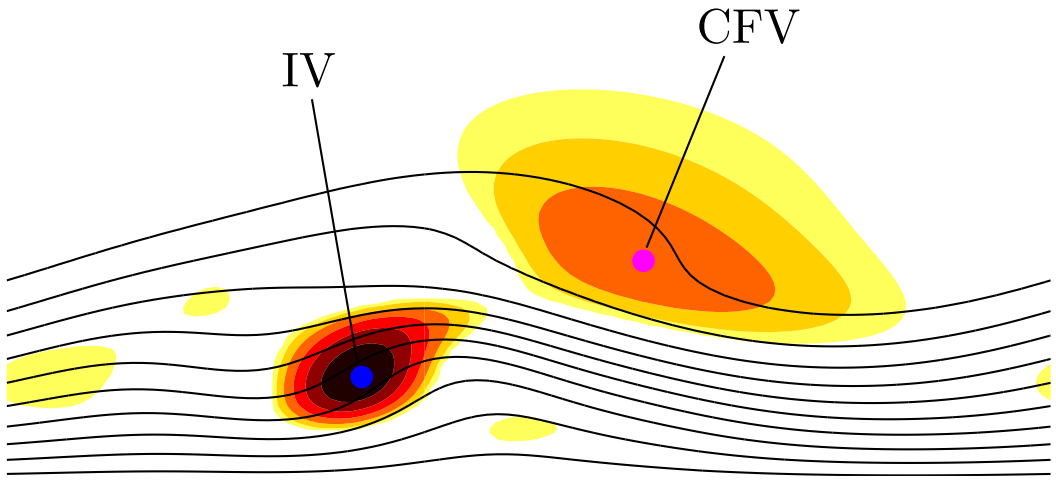
Conclusions

Key outcomes from the stability analysis of swept-wing boundary layers with surface irregularities

3 **Common physical mechanism**

Surface features can generate a counter-rotating vortex in the near-wall crossflow-reversal region.

Weak/absent induced vortex → classical secondary route; strong induced vortex → new highly amplified convective instability.



1 **Predictive framework**

2 **Applicability to surface irregularities**

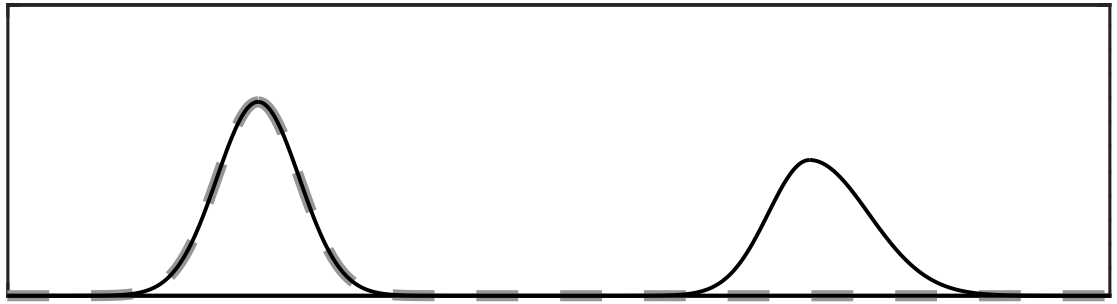
Conclusions

Key outcomes from the stability analysis of swept-wing boundary layers with surface irregularities

4 Passive-control implication

Smooth humps can attenuate stationary-crossflow growth, but no single geometric parameter universally predicts performance.

Double-hump layouts are promising passive-control candidates.



1 Predictive framework

2 Applicability to surface irregularities

3 Common physical mechanism

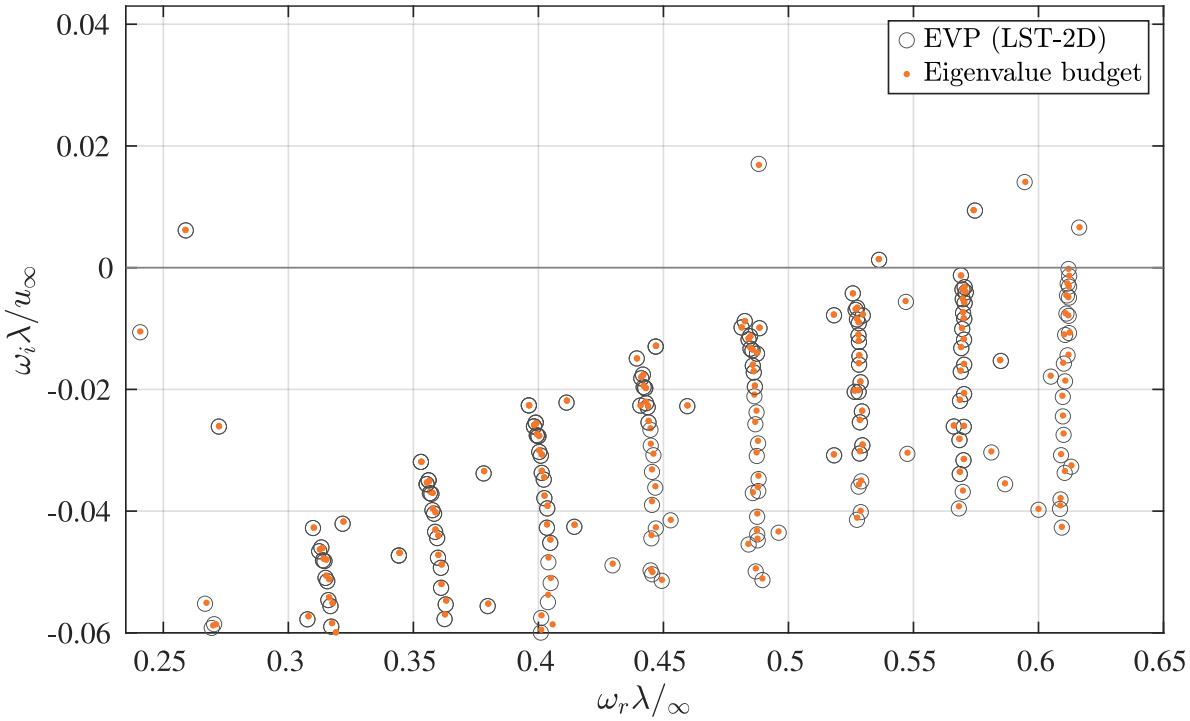
Conclusions

Key outcomes from the stability analysis of swept-wing boundary layers with surface irregularities

5 Eigenvalue-balance framework

A Reynolds–Orr-based eigenvalue balance was derived and verified against LST.

It identifies shear-production, advection and dissipation mechanisms controlling modal growth.



1 Predictive framework

2 Applicability to surface irregularities

3 Common physical mechanism

4 Passive-control implication

Conclusions

Key outcomes from the stability analysis of swept-wing boundary layers with surface irregularities

1 **Predictive framework**

2 **Applicability to surface irregularities**

3 **Common physical mechanism**

4 **Passive-control implication**

5 **Eigenvalue-balance framework**

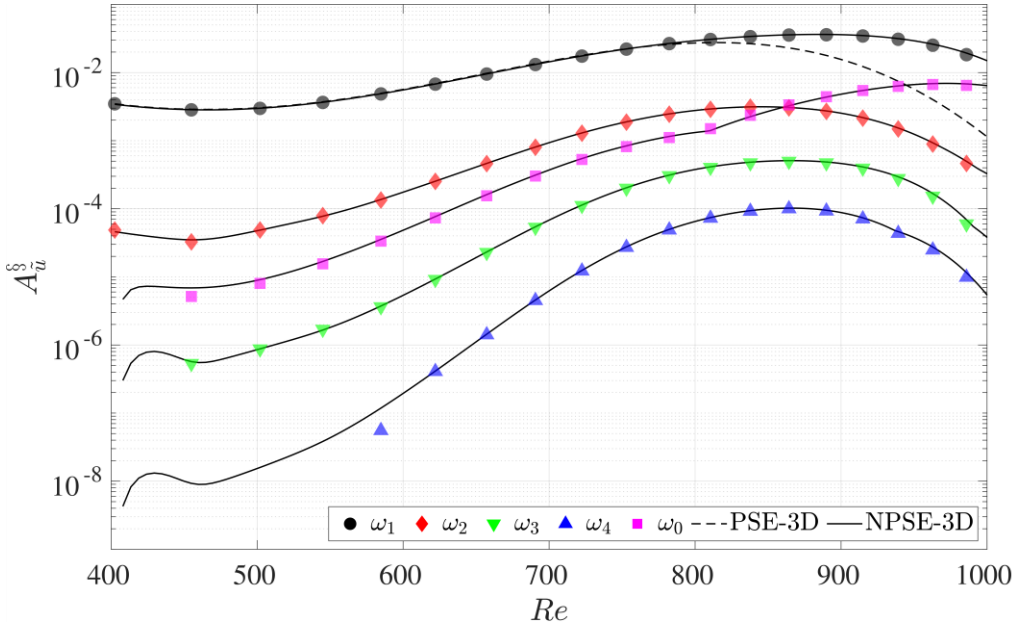
Outlook

Perspectives and future development

1 Non-linear evolution

Apply non-linear PSE-3D to secondary instabilities and instabilities generated by steps, humps and roughness elements.

Outcome: extend the predictive framework toward the nonlinear regime and transition onset



Outlook

Perspectives and future development

1 Non-linear evolution

2 Calibrated transition models

Use DNS/experimental transition data to define critical *N*-factor thresholds for dominant secondary modes.

Outcome: more reliable e^N-type prediction beyond primary-CF correlations.

3 Flight-relevant regimes

Extend the framework to compressible and high-Reynolds-number swept-wing boundary layers.

Outcome: include density, temperature and high-speed effects in stability prediction.

4 Receptivity + shape optimisation

Couple direct/adjoint receptivity analysis with geometry optimisation of humps, wavy walls or distributed features.

Outcome: design surface shapes that weaken instability amplification.

Publications

- Ambrosino B., Tocci, F. Theiβ, A. Rodríguez, D. and Hein, S.: "*Secondary Instabilities of Stationary Crossflow Vortices: Comparison of LST-2D and PSE-3D with DNS*". AIAA Paper 2024-4488, (2024), doi : 10.2514/6.2024-4488 .

- Ambrosino B., Mohammad, M. Kotsonis, M. Hanifi, A. and Hein, S.: "*Stability Analysis on the Effect of a Smooth Surface Hump on Secondary Instabilities of Crossflow Vortices*". 11th European Conference for Aeronautics and Space Sciences, EUCASS Paper FP-514, (2025), doi: 10.13009/EUCASS2025-426 .

- Ambrosino B., Tocci, F. Theiβ, A. Rodríguez, D. and Hein, S.: *"Stationary Crossflow Vortices' Secondary Instability: Linear Stability Theory and Parabolized Stability Equations".* AIAA Journal (2025), doi: 10.2514/1.J064663.

- Ambrosino B., Tocci, F. Theiβ, D. and Hein, S.: *"Numerical Studies on the Influence of Steps in Crossflow-Dominated Boundary Layers".* Under review at Computer & Fluids.

- Ambrosino B., Mohammad, M. Kotsonis, M. Hanifi, A. and Hein, S.: "*Effect of Smooth Surface Hump Geometries on Primary and Secondary Instabilities in Swept-Wing Boundary Layers: Insights from DNS and Linear Stability Analysis*". To be submitted at JFM.

- Ambrosino B., Theiβ, A. and Hein, S.: *"Instability mechanisms in the wake of discrete roughness elements in a swept-wing boundary layer".* To be submitted at JFM.

Thanks for your attention

MARIE SKŁODOWSKA-CURIE ACTIONS
Innovative Training Networks (ITN) Call: H2020-MSCA-ITN-2020
Stability and Sensitivity Methods for Flow Control and Industrial Design (SSECOID)

This project received funding from the European Union's Horizon 2020 research and innovation programme under the Marie Skłodowska-Curie grant agreement No 955923

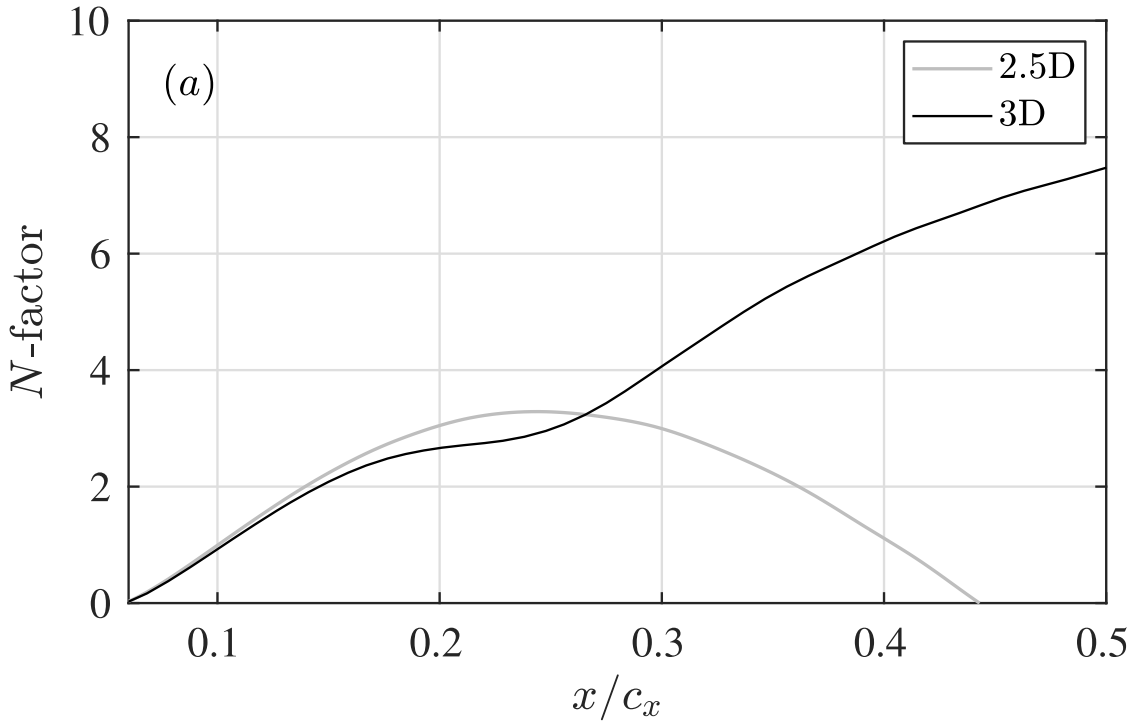
Contact

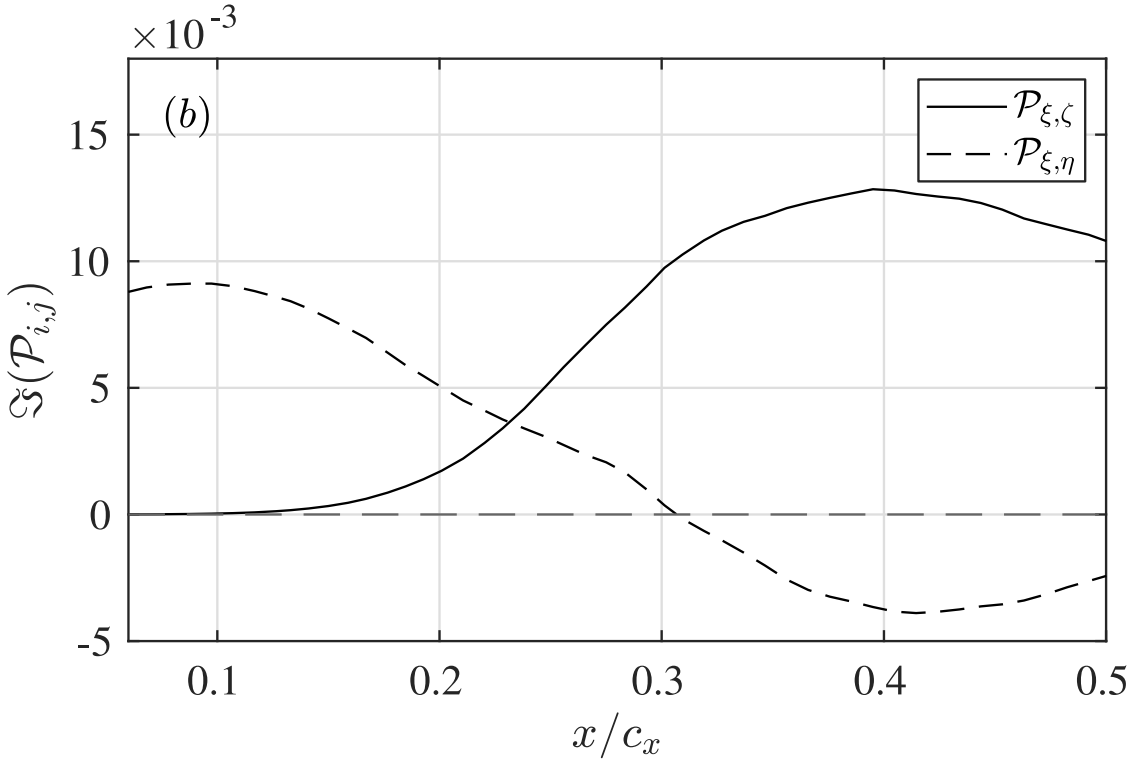
biagio.ambrosino@dlr.de
biagio.ambrosino@alumnos.upm.es

Backup

From primary crossflow instability to secondary instability

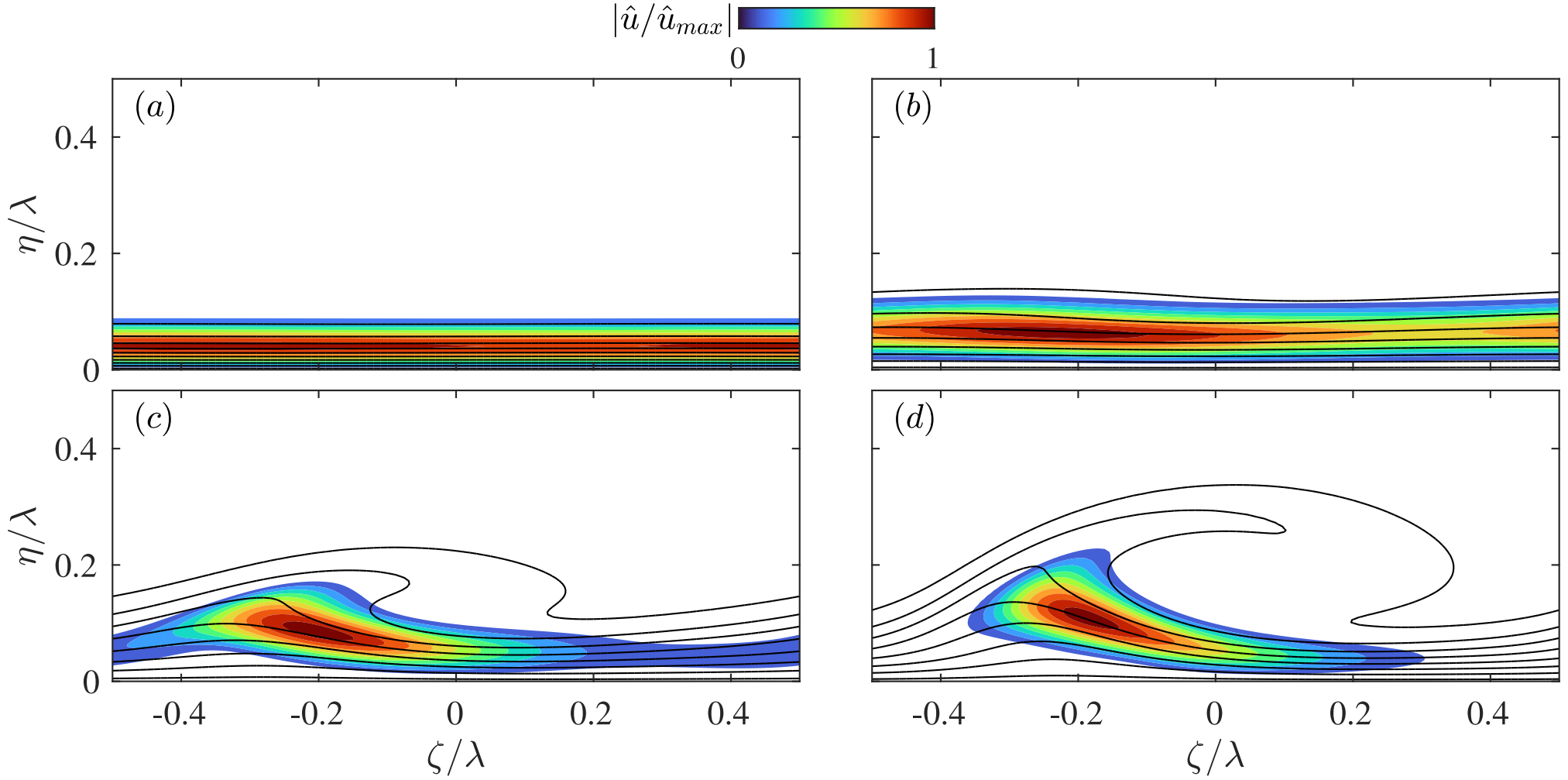
Instability changeover





From primary crossflow instability to secondary instability

Streamwise evolution



NPSE-3D formulation: coupled harmonic evolution

Retaining the nonlinear perturbation terms turns PSE-3D into a harmonic-balance marching problem

FROM SINGLE MODE TO HARMONIC SYSTEM

Truncated temporal Fourier expansion

$$\tilde{\boldsymbol{q}}(\xi,\eta,\zeta,\mathrm{t}) = \sum_{\mathrm{n}=-\mathrm{M}}^{\mathrm{M}} \breve{\mathbf{q}}_n(\xi,\eta,\zeta,)\mathrm{e}^{-in\omega t}$$

PSE scale separation for each harmonic

$$\breve{\mathbf{q}}_n(\xi,\eta,\zeta) = \hat{\boldsymbol{q}}_{\mathrm{n}}(\xi,\eta,\zeta)\, e^{i\int_\xi \alpha_n(\xi')d\xi'}$$

Systems of equation

$$\mathcal{LNS}\left(\sum_n \hat{\boldsymbol{q}}_{\boldsymbol{n}}\, e^{i\left(\int_\xi \alpha_n(\xi')d\xi' - n\omega t\right)}\right)$$
$$= \mathcal{NNS}\left(\sum_p \hat{\boldsymbol{q}}_{\boldsymbol{p}}\, e^{i\left(\int_\xi \alpha_p(\xi')d\xi' - p\omega t\right)} \sum_q \hat{\boldsymbol{q}}_{\boldsymbol{q}}\, e^{i\left(\int_\xi \alpha_q(\xi')d\xi' - q\omega t\right)}\right)$$

f_n contains the nonlinear forcing generated by harmonic interactions

WHAT THE CODE SOLVES

$n = 0$	$n = 1$	$n = 2 \ldots M$
MFD	fundamental	harmonics

Quadratic coupling	harmonic n is forced by all pairs satisfying $p + q = n$
Reality condition	negative harmonics are reconstructed by complex conjugation
Mean-flow distortion	n = 0 represents the steady deformation generated by nonlinear self-interaction

NPSE-3D code workflow: fixed-point marching

At each streamwise station, harmonic fields, nonlinear forcing and wavenumbers are made mutually consistent

STREAMWISE MARCHING

ξ_{i-1} — ξ_i — ξ_{i+1}

PREDICTOR

Initial α_n

Extrapolate from the upstream station

or

local eigenvalue solution at the first station

FIXED-POINT ITERATION AT ξ_i

INNER LOOP — **α_n fixed**

FORCING compute f_n → **HARMONICS** solve $\tilde{q}_n$ → **CHECK** $R_{\tilde{q}_n} \leq \varepsilon_{\tilde{q}_n}$

OUTER LOOP → **PSE NORMALISATION** update α_n

Repeat until both the harmonic fields and wavenumbers converge.

CONVERGED

$\alpha_n \tilde{q}_n$

All retained harmonics satisfy the nonlinear tolerance

MARCH

The forcing terms depend on the disturbance amplitudes themselves → Inner loop on the harmonics